ORGANOMETALLICS
Article

Organometallics **2009,** *28,* 6489–6506 6489
DOI: 10.1021/om900697e

Ion Pairing and Allyl Dynamics in a Series of [Pd(η^3-allyl)(N,N-chelate)](anion) Salts. On the Influence of the BPh_4^- Anion

Aitor Moreno and Paul S. Pregosin*

Laboratory of Inorganic Chemistry, ETHZ, Hönggerberg, CH-8093 Zürich, Switzerland

Beatriz Fuentes

IU CINQUIMA/Quimica Inorganica, Facultad de Ciencias, Universidad de Valladolid, E-47071 Valladolid, Spain

Luis F. Veiros*

Centro de Química Estrutural, Complexo I, Instituto Superior Técnico, Avenida Rovisco Pais 1, 1049-001 Lisbon, Portugal

Alberto Albinati* and Silvia Rizzato

Dipartimento di Chimica Strutturale, Università di Milano, Via G. Venezian 31, 20133 Milano, Italy

Received August 6, 2009

A series of BPh_4^- and other Pd-allyl salts of the form [Pd(η^3-allyl)(N,N-chelate)](anion) (η^3-allyl = $CH_2C(Me)CH_2$, **3**, and PhCHCHCHPh, **4**) have been prepared and studied via PGSE diffusion and other forms of NMR spectroscopy together with X-ray and DFT calculations. The diffusion data reveal that the BPh_4^- salts show a very substantial amount of ion pairing in CD_2Cl_2 solution. Both the solution Overhauser studies and the X-ray results are consistent with a BPh_4^- position that brings one or more phenyl groups very close to the N,N-chelate, and this would facilitate phenylation reactions. Variable-temperature and magnetization transfer NMR measurements reveal allyl and ligand dynamics that fall under the general heading of "apparent rotation". DFT calculations suggest that this isomerization process in **3** and **4** is solvent assisted and proceeds with Pd−N bond breaking.

Introduction

Although many transition metal salts are capable of catalyzing organic transformations, the literature shows that monocationic salts are frequently the catalysts of choice. The selection of the accompanying anion is often restricted to those that are thought to be incapable of competing as a ligand, e.g., BF_4^- or PF_6^- rather than Cl^-. However, the recent literature concerned with anion effects[1−8] in homogeneous catalysis suggests that larger aluminum and boron anions[9] can sometimes afford faster reactions.[10] Thus the tetra phenyl borate derivative $BArF^-$ (= tetra(3,5-ditrifluoromethyl)phenyl borate) is a now often used to accompany the cation. Interestingly, the parent BPh_4^- anion is rarely selected. This may be related to observations in which this anion can form an η^6-arene complex[11] (eq 1) or function as a source of the phenyl anion[12,13] (see eqs 2 and 3).

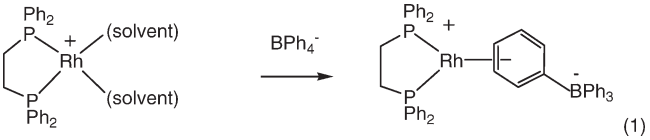

(1)

$$PtH(NO_3)(PEt_3)_2 + Na(BPh_4) \xrightarrow[MeOH]{} Pt(Ph_2)(PEt_3)_2 \quad (2)$$

*Corresponding authors. E-mail: pregosin@inorg.chem.ethz.ch.

(1) Smidt, S. P.; Zimmermann, N.; Studer, M.; Pfaltz, A. *Chem.—Eur. J.* **2004**, *10*, 4685–4693.
(2) Faller, J. W.; Fontaine, P. P. *Organometallics* **2005**, *24*, 4132–4138.
(3) Semeril, D.; Bruneau, C.; Dixneuf, P. H. *Adv. Synth. Catal.* **2002**, *344*, 585–595.
(4) Perez, J.; Riera, L. *Chem Commun.* **2008**, 533–543.
(5) Fagnou, K.; Lautens, M. *Angew. Chem., Int. Ed.* **2002**, *41*, 27–47.
(6) (a) Drago, D.; Pregosin, P. S.; Pfaltz, A. *Chem. Commun.* **2002**, 286–287. (b) Martinez-Viviente, E.; Pregosin, P. S. *Inorg. Chem.* **2003**, *42*, 2209–2214. (c) Kumar, P. G. A.; Pregosin, P. S.; Schmid, T. M.; Consiglio, G. *Magn. Reson. Chem.* **2004**, *42*, 795–800. (d) Macchioni, A. *Chem. Rev.* **2005**, *105*, 2039–2073.
(7) Evans, D. A.; Murry, J. A.; von Matt, P.; Norcross, R. D.; Miller, S. J. *Angew. Chem., Int. Ed. Engl.* **1995**, *34*, 798.
(8) Burckhardt, U.; Baumann, M.; Togni, A. *Tetrahedron: Asymmetry* **1997**, *8*, 155.
(9) Krossing, I.; Raabe, I. *Angew. Chem., Int. Ed.* **2004**, *43*, 2066–2090.
(10) Kundig, E. P.; Saudan, C. M.; Bernardinelli, G. *Angew. Chem., Int. Ed.* **1999**, *38*, 1220.
(11) (a) Aresta, M.; Quaranta, E.; Albinati, A. *Organometallics* **1993**, *12*, 2032–2043. (b) Torres, F.; Sola, E.; Martin, M.; Ochs, C.; Picazo, G.; Lopez, J. A.; Lahoz, F. J.; Oro, L. *Organometallics* **2001**, *20*, 2716–2724. (c) Note that BArF can also form an η^6-complex: Douglas, T. M.; Molinos, E.; Brayshaw, S. K.; Weller, A. S. *Organometallics* **2007**, *26*, 463–465.
(12) (a) Deeming, A. J.; Johnson, B. F. G.; Lewis, J. J. *J. Chem. Soc., Dalton Trans.* **1973**, 1848. (b) Zheng, S.; Xu, L.; Xia, C. *Appl. Organomet. Chem.* **2007**, *21*, 772–776.
(13) Siegmann, K.; Pregosin, P. S.; Venanzi, L. M. *Organometallics* **1989**, *8*, 2659–2664.

Published on Web 10/19/2009

12a

$$PtH(NO_3)(PEt_3)_2 + Na(BPh_4) \xrightarrow[MeOH]{} (PEt_3)_2HPt(\mu\text{-}H)Pt(Ph)(PEt_3)_2^+ \quad (3)$$

13

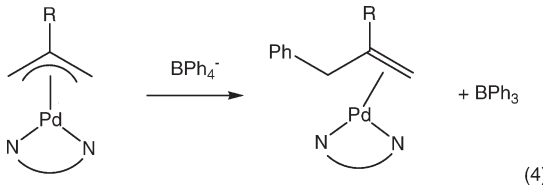

(4)

Some time ago Crociani and co-workers[14] reported on the phenylation of palladium-allyl cationic complexes (see eq 4) and suggested that the BPh_4^- anion might well be involved in extensive ion pairing. In our NMR studies on cationic $Mn(CO)_3(\eta^6\text{-arene})^+$ complexes[15] with several boron counterions using pulsed gradient spin−echo (PGSE) NMR diffusion methods[16] we could show that, indeed, there was much more ion pairing with BPh_4^- than with $BArF^-$. A similar finding was reported for $Ru(\eta^6\text{-arene})$ salts bearing α-diimine ligands.[17]

Since we have a long-standing interest in palladium allyl complexes,[18] we have prepared some old and new salts of the form [Pd(η^3-allyl)(N,N)](anion) (see Scheme 1) and report here studies concerned with the nature of the ionic interactions and aspects of their dynamics in CD_2Cl_2 solutions. The NMR approach to the subject of ion pairing follows that used in our earlier studies.[16,19] We separately measure the diffusion constants (*D* values) for the cation and anion. If these are identical and lead to relatively large hydrodynamic radii, r_H, we conclude that there is approximately 100% ion pairing. This will often be the case for $CDCl_3$ solutions; however, for other solvents, for example, CD_2Cl_2, one normally finds intermediate ion pairing. We then use $^{19}F,^1H$ (or $^1H,^1H$) Overhauser measurements to provide insight into the structure of the ion pair and try to support these solution results with both X-ray crystallography and DFT calculations. In addition to the question of ion pairing we also consider aspects of the allyl dynamics in our salts.

Results and Discussion

Scheme 1 shows the two η^3-allyl ligand types selected. Several model salts contain either the $BArF^-$ or PF_6^- anions in addition to those with the BPh_4^- anion. The new Pd-allyl cationic complexes **3** and **4** were prepared using standard methods (see Experimental Section) and were characterized via NMR and microanalytical methods in addition to five X-ray diffraction studies. Many of the BPh_4^- salts decompose at room temperature, due to the phenylation reaction mentioned above, so that the characterization for these salts required low-temperature measurements.

Table 1 shows ^{13}CNMR data for the allyl carbons of the salts. These NMR parameters have been reported on a number of occasions[18,20−24] and used in discussions of both bonding and reactivity. For the 2-methyl allyl cations, **3**, the terminal allyl ^{13}C signals fall in the range $\delta = 61-64$, and we do not find marked changes in their positions when the two N-donors are different. The 1,3-diphenyl allyl cationic salts, **4**, show the terminal allyl carbons in the range $\delta = 78-81$, in agreement with the literature.[18] In all of these complexes, changing the anion has little or no effect on these allyl carbon ^{13}C chemical shifts. Moreover, there are no noteworthy changes in these terminal allyl ^{13}C values when the chelating ligands contain bulky groups in the *ortho* positions of the Schiff base rings.

Interestingly, a comparison of the ^1H chemical shifts for the PF_6^- and BPh_4^- salts shows that many protons in the latter salts are shifted to lower frequency. Presumably this is due to the local anisotropic effects associated with a proximate B(Ph) moiety (see Scheme 2 and Scheme S1). The largest changes are found in the N,N-chelate rings, and the same comparison using PF_6^- and $BArF^-$ (rather than BPh_4^-) reveals only small differences, suggesting that the $BArF^-$ is not as strongly ion paired as BPh_4^-.

X-ray Diffraction Studies. Five of the palladium salts proved amenable for structural studies, and Table 2 provides a list of the experimental details associated with these measurements. Figure 1 shows ORTEP plots for the four 2-methyl allyl cations, **3a**, **3b**, **3f** (as BPh_4^- salts) and **3h** (as a PF_6^- salt). Figure 2 gives the corresponding view for the 1,3-diphenyl cation, **4g** (as a PF_6^- salt). The immediate coordination spheres about the palladium atoms consist of the two N-donors and the η^3-allyl ligand. The complexed 2-methyl allyl ligand is distorted such that the methyl group is tipped

(14) Crociani, B.; Antonaroli, S.; Dibianca, F.; Fontana, A. *J. Organomet. Chem.* **1993**, *450*, 21–26.
(15) Schott, D.; Pregosin, P. S.; Jacques, N.; Chavarot, M.; Rose-Munch, F.; Rose, E. *Inorg. Chem.* **2005**, *44*, 5941–5948.
(16) (a) Pregosin, P. S. *Prog. Nucl. Magn. Reson. Spectrosc.* **2006**, *49*, 261–288. (b) Pregosin, P. S.; Kumar, P. G. A.; Fernandez, I. *Chem. Rev.* **2005**, *105*, 2977–2998. (c) Kumar, P. G. A. *Aust. J. Chem.* **2006**, *59*, 78–78.
(17) (a) Zuccaccia, D.; Bellachioma, G.; Cardaci, G.; Ciancaleoni, G.; Zuccaccia, C.; Clot, E.; Macchioni, A. *Organometallics* **2007**, *26*, 3930. (b) Binotti, B.; Bellachioma, G.; Cardaci, G.; Carfagna, C.; Zuccaccia, C.; Macchioni, A. *Chem.−Eur. J.* **2007**, *13*, 1570. (c) Zuccaccia, D.; Macchioni, A. *Organometallics* **2005**, *24*, 3476. (d) Macchioni, A.; Bellachioma, G.; Cardaci, G.; Travaglia, M.; Zuccaccia, C.; Milani, B.; Corso, G.; Zangrando, E.; Mestroni, G.; Carfagna, C.; Formica, M. *Organometallics* **1999**, *18*, 3061.
(18) (a) Pregosin, P. S.; Salzmann, R. *Coord. Chem. Rev.* **1996**, *155*, 35–68. (b) Barbaro, P.; Pregosin, P. S.; Salzmann, R.; Albinati, A.; Kunz, R. W. *Organometallics* **1995**, *14*, 5160. (c) Herrmann, J.; Pregosin, P. S.; Salzmann, R.; Albinati, A. *Organometallics* **1995**, *14*, 3311. (d) Pregosin, P. S.; Rüegger, H. *Magn. Reson. Chem.* **1994**, *32*, 297–302. (e) Pregosin, P. S.; Ruegger, H.; Salzmann, R.; Albinati, A.; Lianza, F.; Kunz, R. W. *Organometallics* **1994**, *13*, 5040–5048. (f) Pregosin, P. S.; Ruegger, H.; Salzmann, R.; Albinati, A.; Lianza, F.; Kunz, R. W. *Organometallics* **1994**, *13*, 83–90.
(19) (a) Moreno, A.; Pregosin, P. S.; Veiros, L. E.; Albinati, A.; Rizzato, S. *Chem.−Eur. J* **2008**, *14*, 5617–5629. (b) Schott, D.; Pregosin, P. S.; Albinati, A.; Rizzato, S. *Inorg. Chim. Acta* **2007**, *360*, 3203–3212. (c) Fernandez, I.; Pregosin, P. S.; Albinati, A.; Rizzato, S. *Organometallics* **2006**, *25*, 4520–4529. (d) Nama, D.; Schott, D.; Pregosin, P. S.; Veiros, L. F.; Calhorda, M. J. *Organometallics* **2006**, *25*, 4596–4604.
(20) Åkermark, B.; Krakenberger, B.; S., H.; Vitagliano, A. *Organometallics* **1987**, *6*, 620.
(21) (a) Henning, S.; Reggelin, M.; Helmchen, G. *Angew. Chem.* **1997**, *109*, 2199–2202. (b) Kollmar, M.; Goldfuss, B.; Reggelin, M.; Rominger, F.; Helmchen, G. *Chem.−Eur. J.* **2001**, *7*, 4913–4927. (c) Kollmar, M.; Helmchen, G. *Organometallics* **2002**, *21*, 4771–4775.
(22) (a) Malet, R.; Moreno-Manas, M.; Pajuelo, F.; Parella, T.; Pleixats, R. *Magn. Reson. Chem.* **1997**, *35*, 227–236. (b) Malet, R.; Moreno-Manas, M.; Parella, T.; Pleixats, R. *Organometallics* **1995**, *14*, 2463–2469.
(23) (a) Lloyd-Jones, G. C.; Stephen, S. C.; Murray, M.; Butts, C. P.; Vyskocil, S.; Kocovsky, P. *Chem.−Eur. J.* **2000**, *6*, 4348–4357. (b) Normand, A. T.; Stasch, A.; Ooi, L. L.; Cavell, K. J. *Organometallics* **2008**, *27*, 6507–6520.
(24) (a) von Matt, P.; Lloyd-Jones, G. C.; Minidis, A. B. E.; Pfaltz, A.; Macko, L.; Neuburger, M.; Zehnder, M.; Rüegger, H.; Pregosin, P. S. *Helv. Chim. Acta* **1995**, *78*, 265. (b) Pregosin, P. S.; Salzmann, R.; Togni, A. *Organometallics* **1995**, *14*, 842–847.

Scheme 1

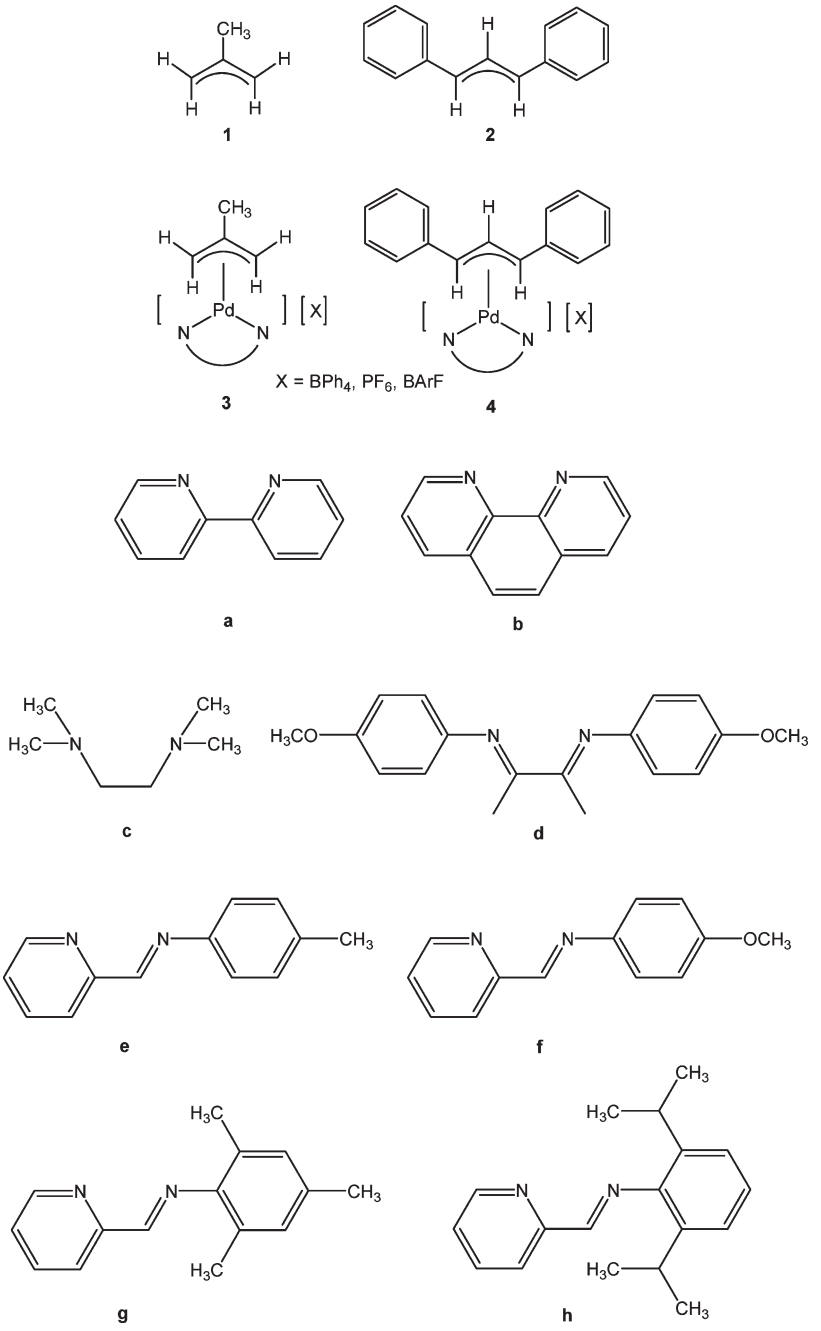

away from the Pd center, in keeping with earlier measurements on this type of ligand.[25]

The N−Pd−N chelate angles are all normal at ca. 78−79°. The Pd−N bond lengths for the nitrogen ligands in the complexed allyl salts fall in the relatively narrow range ca. 2.09−2.13 Å. We note that in cation **4g**, where some steric crowding is unavoidable, the Pd−N(pyr) bond length, Pd(1)−N(1′), 2.129(4) Å, is slightly longer than that for the Schiff base Pd−N interaction, Pd(1)−N(1), 2.091(4) Å. For the four 2-methyl allyl salts, the various Pd−C(terminal allyl) separations do not vary much and mostly fall in the range 2.10−2.15 Å.

For **3a** and **3b** the positions of the BPh_4^- anions with respect to the cation are informative, and these are shown in Figure 3. There are a few short contacts between the BPh_4^- anions and the Pd cationic complexes in the range 2.7−2.9 Å, both in **3a**(BPh_4) and **3b**(BPh_4), the other packing distances being longer than 3 Å. It is interesting to notice that in both

(25) For Pd(2-methyl allyl) structures, see: (a) Deeming, A. J.; Rothwell, I. P.; Hursthouse, M. B.; Malik, K. M. A. *J. Chem. Soc., Dalton Trans*. **1979**, 1899–1911. (b) Albinati, A.; Kunz, R. W.; Ammann, C. J.; Pregosin, P. S. *Organometallics* **1991**, *10*, 1800–1806. (c) Ozawa, F.; Son, T. I.; Ebina, S.; Osakada, K.; Yamamoto, A. *Organometallics* **1992**, *11*, 171–176. (d) Fernandez-Galan, R.; Manzano, B. R.; Otero, A.; Lanfranchi, M.; Pellinghelli, M. A. *Inorg. Chem*. **1994**, *33*, 2309–2312. (e) Delis, J. G. P.; Groen, J. H.; Vrieze, K.; van Leeuwen, P.; Veldman, N.; Spek, A. L. *Organometallics* **1997**, *16*, 551–562. (f) Danopoulos, A. A.; Tsoureas, N.; Macgregor, S. A.; Smith, C. *Organometallics* **2007**, *26*, 253–263. For Pd(1,3-diphenyl allyl) structures, see: (g) Barbaro, P.; Pregosin, P. S.; Salzmann, R.; Albinati, A.; Kunz, R. *Organometallics* **1995**, *14*, 5160–5170. (h) Bastero, A.; Bella, A. F.; Fernandez, F.; Jansat, S.; Claver, C.; Gomez, M.; Muller, G.; Ruiz, A.; Font-Bardia, M.; Solans, X. *Eur. J. Inorg. Chem*. **2007**, 132–139. (i) Ferioli, F.; Fiorelli, C.; Martelli, G.; Monari, M.; Savoia, D.; Tobaldin, P. *Eur. J. Org* **2005**, 1416–1426.

compounds a tetraphenyl borate anion is placed opposite the η^3-allyl moiety and close to the nitrogen chelate ring (cf. Figure 3), in agreement with the solution NMR data (see below); this may result, in part, from the partial positive charges arising when the N atoms coordinated to the Pd atom. We note that in **3a**(BPh_4) the anion intrudes much more into the space occupied by the N,N-chelate than in **3b**(BPh_4). This observation seems to be related to a modest distortion in the allyl bonding.

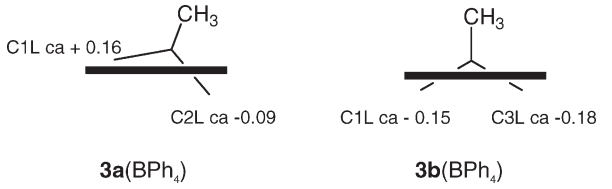

3a(BPh_4) **3b**(BPh_4)

In **3a**(BPh_4) the allyl is slightly rotated with respect to the N−Pd−N plane (indicated as a solid black line), whereas in **3b**(BPh_4) the two terminal allyl carbons are both slightly below this plane. There is a similar modest rotation in the 1,3-diphenyl salt **4g**(PF_6).

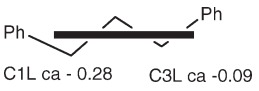

Summarizing these solid-state results, we find that the "short" anion−cation interactions observed in the solid state (e.g., ≤2.8 Å for the BPh_4^- complexes and ≤2.6 Å for the PF_6^- anions) are consistent with the contacts found in solution.

Diffusion Results. In addition to the new diffusion data for the η^3-allyl salts shown in Scheme 1 (see Table 3), we have already collected a relatively large number of diffusion constants (D values) for CD_2Cl_2 solutions of organic and inorganic PF_6^- salts[19a,b] (including some with η^3-allyl ligands[26]). These data all arise from pulsed gradient spin−echo (PGSE) NMR measurements. As noted above, one normally finds intermediate ion pairing in this solvent, but the hydrodynamic radii that are calculated from the Stokes−Einstein equation[27] suggest that the ions are larger than what might be expected for acetone or aqueous solutions. For example, the D values for the ions of **3a**(PF_6), (13.02 for the cation and 13.54 for the anion) are not identical, but the corrected hydrodynamic radius of 4.9 Å for the anion is too large for a simple solvated PF_6^- anion. Further, the D (and r_H) values in **3a**(PF_6) for the cation and anion in the more polar solvent acetone (15.64 (5.4 Å) and 24.80 (4.4 Å), respectively) confirm that the smaller anion is indeed diffusing much faster than the cation. Therefore, the larger r_H value of 4.9 Å for the anion in CD_2Cl_2 is consistent with intermediate ion pairing.

Table 1. ^{13}C NMR Data for the Allyl Groups in Compounds 3 and 4 in CD_2Cl_2

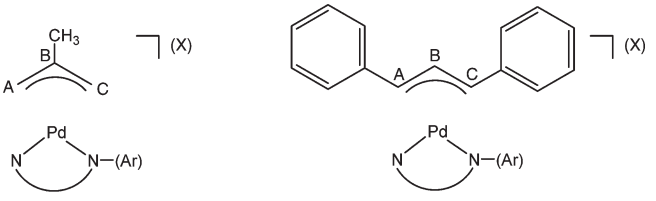

3 **4**

cation	X	T/K	A	B	C
3a	PF_6	298	61.1	136.9	
	BPh_4	298	61.1	136.7	
	BArF	298	61.4	137.5	
3b	PF_6	298	61.0	136.7	
	BPh_4	298	61.0	136.6	
3c	BPh_4	298	60.1	135.5	
3d	BPh_4	213	64.3	136.8	
3e	BPh_4	253	62.2	136.4	63.9
3f	BPh_4	213	61.9	135.9	63.2
3g	PF_6	263	61.8	136.6	62.2
	BPh_4	263	61.5	136.5	62.2
	BArF	263	61.6	137.6	62.7
3h	PF_6	263	61.8	137.2	62.8
	BPh_4	263	62.1	137.4	63.3
	BArF	223	61.6	137.4	63.3
4e	PF_6	193	81.2	108.4	77.7
	BPh_4	193	81.2	108.1	77.7
4g	PF_6	223	80.1	106.8	78.1
	BPh_4	223	79.6	106.8	78.0
	BArF	263	80.5	106.8	79.0
4h	PF_6	263	80.5	106.3	79.0
	BPh_4	263	80.6	106.2	78.6
	BArF	203	80.6	106.3	78.3

For the analogous salt **3a**(BArF), $D = 12.32$ for the cation and $D = 8.48$ for the anion with $r_H^{corr} = 6.8$ Å; these data suggest some but not much ion pairing since the corrected r_H for BArF is known to be ca. 6.6 Å. Only three BPh_4^- salts, **3a**−**3c**, are stable at ambient temperature, and once again the diffusion data suggest intermediate ion pairing at 299 K. For example, the D value for the cation of the **3a** analogue is 12.32 and that for the anion 10.40.

Before discussing the 263 K D values for the more reactive salts, three effects that drastically affect the measured D values need to be considered: (a) possible convection,[28] (b) solution viscosity[29a] (due to the change in temperature from 299 to 263 K), and (c) solvent dielectric constant[29b] (again due to the change in temperature). We have suggested a method[28] of suppressing convection and thereby obtaining reliable D values at low temperature. This procedure requires

(26) Schott, D.; Pregosin, P. S.; Veiros, L. F.; Calhorda, M. J. *Organometallics* **2005**, *24*, 5710–5717.

(27) The measured D value can be used to solve the Stokes−Einstein relation, $r_H = kT/6\pi\eta D$, for the hydrodynamic radius, r_H. However, this relation has been subject to criticism, in that the value 6 is often too large; see: (a) Zuccaccia, D.; Macchioni, A. *Organometallics* **2005**, *24*, 3476−3486. An empirical correction to afford r_H^{corr} has been suggested; see: (b) Macchioni, A.; Ciancaleoni, G.; Zuccaccia, C.; Zuccaccia, D. *Chem. Soc. Rev.* **2008**, *37*, 479.

(28) Martinez-Viviente, E.; Pregosin, P. S. *Helv. Chim. Acta* **2003**, *86*, 2364–2378.

(29) (a) Yaws, C. L. *Chemical Properties Handbook*; McGraw-Hill, 1999; pp 478−480. (b) *Handbook of Chemistry & Physics*, 89th ed., 2008−2009 (online).

(30) (a) Ciancaleoni, G.; Zuccaccia, C.; Zuccaccia, D.; Clot, E.; Macchioni, A. *Organometallics* **2009**, 960–967. (b) Ciancaleoni, G.; Zuccaccia, C.; Zuccaccia, D.; Macchioni, A. *Magn. Reson. Chem.* **2008**, *46*, S72–S79. (c) Bellachioma, G.; Ciancaleoni, G.; Zuccaccia, C.; Zuccaccia, D.; Macchioni, A. *Coord. Chem. Rev.* **2008**, *252*, 2224–2238. (d) Rocchigiani, L.; Zuccaccia, C.; Zuccaccia, D.; Macchioni, A. *Chem.−Eur. J.* **2008**, *14*, 6589–6592. (e) Zuccaccia, D.; Foresti, E.; Pettirossi, S.; Sabatino, P.; Zuccaccia, C.; Macchioni, A. *Organometallics* **2007**, *26*, 6099–6105. (f) Ciancaleoni, G.; Di Maio, I.; Zuccaccia, D.; Macchioni, A. *Organometallics* **2007**, *26*, 489–496. (g) Zuccaccia, D.; Bellachioma, G.; Cardaci, G.; Zuccaccia, C.; Macchioni, A. *Dalton Trans.* **2006**, 1963–1971.

Scheme 2. Two Examples of Differences in ^{1}H Chemical Shifts ($\Delta\delta$ (PF_6^- − BPh_4)) between PF_6^- and BPh_4^- Salts ($\Delta\delta$ values, given in ppm)

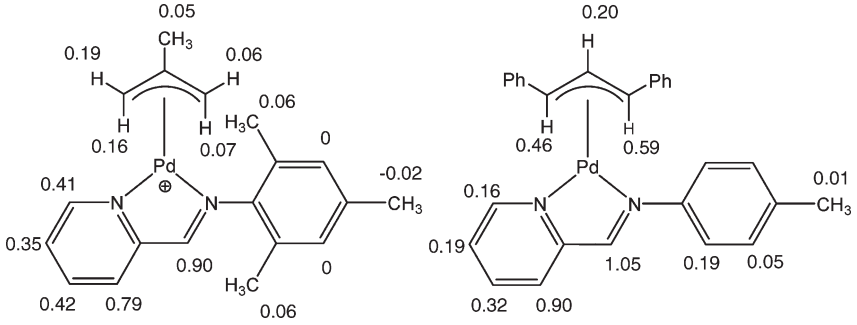

Table 2. Experimental Data for the X-ray Diffraction Study of Compounds 3a(BPh_4), 3b(BPh_4), 3f(BPh_4), 3h(PF_6), and 4g(PF_6)·(Et_2O)

	3a [BPh_4]	**3b** [BPh_4]	**3f** [BPh_4]	**3h** [PF_6]	**4g** [PF_6]·(Et_2O)
formula	$C_{38}H_{35}BN_2Pd$	$C_{40}H_{35}BN_2Pd$	$C_{41}H_{39}BN_2OPd$	$C_{22}H_{29}F_6N_2PPd$	$C_{32}H_{34}F_6N_2O_{0.5}PPd$
mol wt	636.89	660.91	692.95	572.84	705.98
data coll T, K	150(2)	150(2)	295(2)	150(2)	295(2)
diffractometer			Bruker APEX II CCD		
cryst syst	monoclinic	triclinic	monoclinic	orthorhombic	triclinic
space group (no.)	$C2/c$ (15)	$P\bar{1}$ (2)	$P2_1/n$ (14)	$P2_12_12_1$ (19)	$P\bar{1}$ (2)
a, Å	21.526(1)	11.341(1)	9.7435(6)	8.2983(6)	10.5449(9)
b, Å	13.4110(6)	12.287(1)	24.092(2)	10.1408(7)	15.848(1)
c, Å	22.919(1)	13.584(2)	14.5385(9)	28.891(2)	19.611(2)
α, deg	90.	115.187(1)	70.635(1)	90.	79.266(1)
β, deg	110.205(1)	112.844(1)	79.001(1)	90.	85.419(1)
γ, deg	90.	90.092(1)	77.229(1)	90.	81.359(1)
V, Å^3	6209.2(5)	1546.5(3)	3391.5(4)	2431.2(3)	3179.0(5)
Z	8	2	4	4	4
$\rho_{(calcd)}$, g cm^{-3}	1.363	1.419	1.357	1.565	1.475
μ, mm^{-1}	0.627	0.632	0.582	0.887	0.695
radiation	Mo Kα (graphite monochromated, $\lambda = 0.71073$ Å)				
θ range, deg	$1.82 \le \theta \le 28.32$	$1.87 \le \theta \le 27.23$	$2.20 \le \theta \le 28.39$	$2.13 \le \theta \le 29.28$	$1.83 \le \theta \le 28.37$
no. data collected	36 973	18 083	41 790	14 203	39 805
no. indep data	7704	6845	8421	5869	15 461
no. obsd reflns (n_o) [$\lvert F_o\rvert^2 > 2.0\sigma(\lvert F\rvert^2)$]	5748	4428	5859	5597	10 356
no. of params refined (n_v)	484	442	430	301	757
absolute struct param [Flack param]				0.01(2)	
R_{int}	0.0575	0.0546	0.0433	0.0225	0.0278
R (obsd reflns)	0.0381	0.0276	0.0368	0.0260	0.0625
R_w^2 (obsd reflns)	0.0762	0.0860	0.0859	0.0584	0.1763
GOF[d]	1.045	1.003	0.999	1.022	1.019

[a] $R_{int} = \sum\lvert F_o^2 - \langle F_o^2\rangle\rvert/\sum F_o^2$. [b] $R = \sum(\lvert F_o - (1/k)F_c\rvert)/\sum\lvert F_o\rvert$. [c] $R_w^2 = \{\sum[w(F_o^2 - (1/k)F_c^2)^2]/\sum w\lvert F_o^2\rvert^2]\}^{1/2}$. [d] $GOF = [\sum_w(F_o^2 - (1/k)F_c^2)^2/(n_o - n_v)]^{1/2}$.

placing the sample solution in a capillary surrounded by another (or no) solvent. Given the relatively small amount of CD_2Cl_2 solution measured, there is a significant reduction in the signal-to-noise with the result that higher concentrations are often necessary. It is well known[30] that increasing the sample concentration (in our case from 2 to 10 mM) will result in some salt aggregation. The dependence of both viscosity and dielectric constant on temperature is known,[29] and we have corrected for the first in the calculations of the r_H values. It is important for this discussion to realize that CD_2Cl_2 and other solvents are *more polar* at lower temperature so that one might expect less ion pairing.

To obtain an idea of the effect on the D values of changing from 2 to 10 mM solutions, we show data in Table 3 for three salts (entries 11−13) at this higher concentration at 299 K. For **3a**(PF_6) the 10 mM D values are now 12.65 and 13.32, whereas previously these were 13.02 and 13.54, for the cation and anion, respectively. The table also shows a set of model measurements for 10 mM solutions of PF_6^- and $BArF^-$ at 263 K (entries 14−19), at which temperature the BPh_4^- salts are stable for prolonged periods. The D values are now all markedly smaller (primarily due to the change in viscosity); however, once again, the two D values for the cation and anion within any one salt are not identical.

Entries 20−30 show the diffusion data for the 10 mM solutions of the BPh_4^- salts at 263 K. For the two stable salts, **3a**(BPh_4) and **3c**(BPh_4), entries 20 and 21, the two D values for the cation and anion are not identical. However, for the more reactive salts, entries 22−30, the two D values are either very much closer or identical within the experimental error. Even allowing for the possibility that, by coincidence, the cation and anion might have similar sizes, the much larger r_H^{corr} values, 6.3−6.9 Å, confirm that there is now a very substantial amount of ion pairing. *Indeed, in some cases the ion pairing appears to be 100% despite the increase in dielectric constant due to the lower temperature*. To support this conclusion, we have made a few (time-consuming) low-temperature measurements at 2 mM (entries 31−37) and find

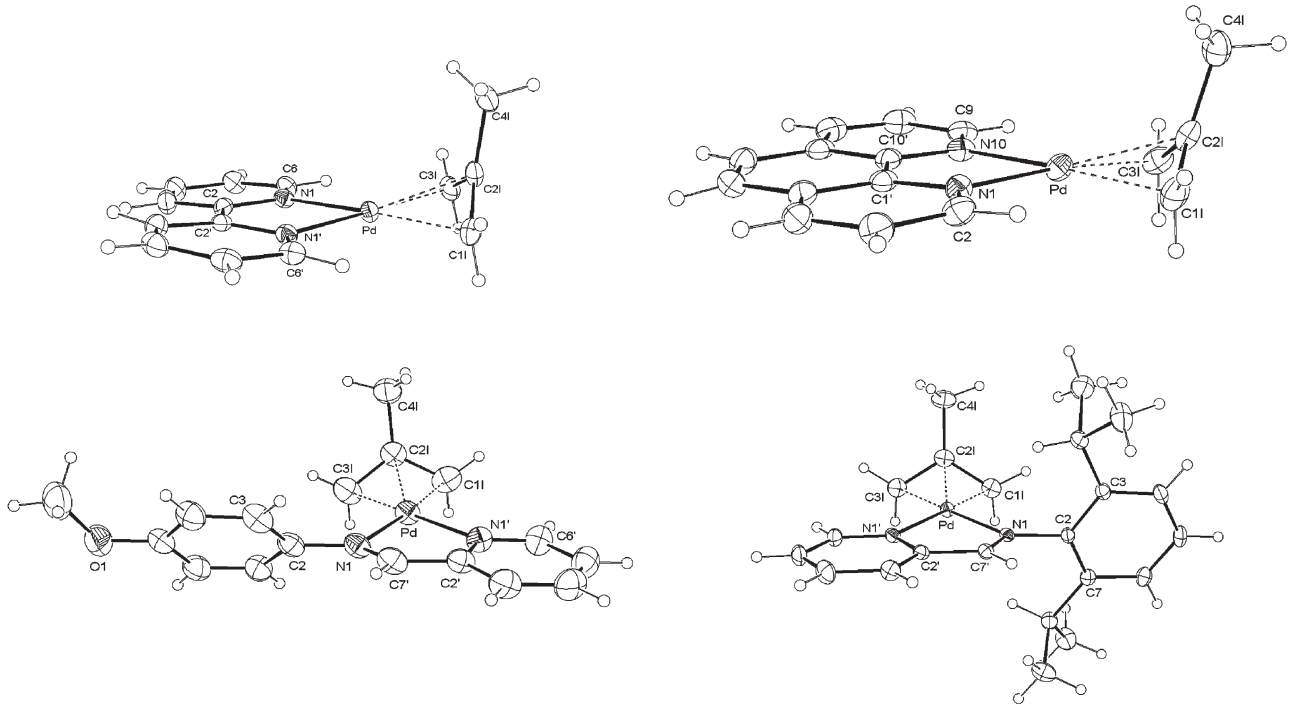

Figure 1. ORTEP plots for the four 2-methyl allyl cations, **3a** and **3b**. Ellipsoids are drawn at 50% probability. Selected bond lengths (Å) and bond angles (deg) for the cations in **3a**: Pd−N(1), 2.089(2); Pd−N(1′), 2.107(2); Pd−C(1L), 2.126(3); Pd−C(2L), 2.133(3); Pd−C(3L), 2.112(3); N(1)−Pd−N(1′) 78.72(7). The average B−C separation is 1.650(5). **3b**: Pd−N(1), 2.099(3); Pd−N(10), 2.102(3); Pd−C(1L), 2.118(5); Pd−C(2L), 2.146(4); Pd−C(3L), 2.091(5); N(1)−Pd−N(10) 79.1(1). The average B−C separation is 1.645(4). **3f**: Pd−N(1′), 2.108(2); Pd−N(1), 2.127(2); Pd−C(1L), 2.108(3); Pd−C(2L), 2.143(2); Pd−C(3L), 2.111(3); N(1′)−Pd−N(1), 78.28(8). The average B−C separation is 1.644(5). **3h**: Pd−N(1), 2.100(2); Pd−N(1′), 2.108(2); Pd−C(1L), 2.115(3); Pd−C(2L), 2.149(3); Pd−C(3L), 2.119(3); N(1)−Pd−N(1′) 78.63(8).

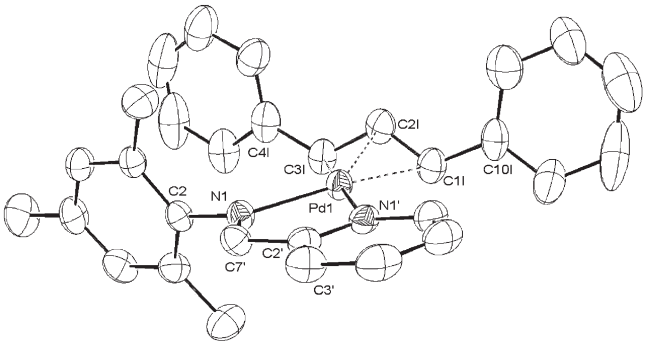

Figure 2. ORTEP plot for the 1,3-diphenyl cation, **4g**. Ellipsoids are drawn at 50% probability; hydrogen atoms omitted for clarity. Selected bond lengths (Å) and bond angles (deg) for one of the two independent cations in **4g**: Pd(1)−N(1), 2.091(4); Pd(1)−N(1′), 2.129(4); Pd(1)−C(1L); 2.159(5); Pd(1)−C(2L), 2.138(5); Pd(1)−C(3L), 2.160(5); N(1)−Pd(1)−N(1′), 77.8(1).

that the reactive BPh_4^- salts are still very strongly ion paired. For example, for the 1,3-diphenyl allyl salt **4g**(BPh_4), the two *D* values are (5.67 and 5.72 for the anion and cation, respectively) now identical within the experimental error.

We conclude that several of the BPh_4^- salts do indeed show more ion pairing in CD_2Cl_2 solution relative to, for example, the $BArF^-$ analogues, in agreement with Crociani's suggestion. Further, the X-ray studies suggest that the BPh_4^- anion is indeed quite close to the Pd atom, and it now remains to consider the interaction of the ions in solution.

Anion/Cation Interactions. The ^{19}F,^{1}H HOESY spectra for the allyl complexes **3** and **4** with PF_6^- as model anion show

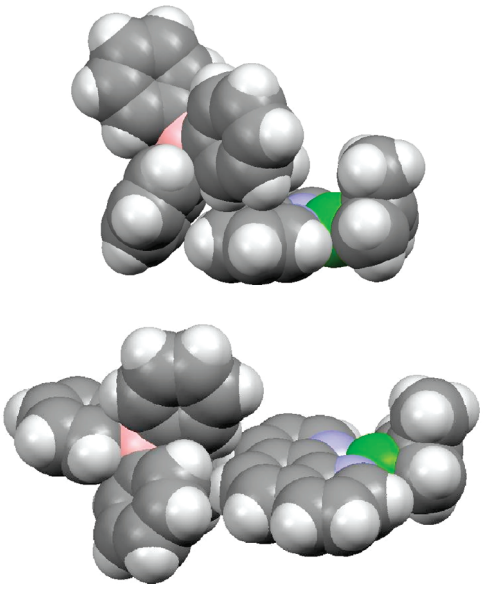

Figure 3. Positions of the BPh_4^- anions in **3a**(BPh_4) (top) and **3b**(BPh_4) (bottom).

an interesting general picture. There are a relatively large number of interionic contacts (five or more in every salt), and *both* the allyl and the N,N-chelate are involved.

For all of the 2-methyl allyl salts, **3**, one observes modest to strong contacts to *all* of the allyl protons including the methyl group, with the *syn* allyl proton the strongest within this ligand. In these simple allyl salts the various contacts to

Table 3. D (10^{-10} m^2 s^{-1}) and r_H (Å) Values[a] for [Pd(η^3-allyl)(N−N)](X) in CD_2Cl_2 at 299 and 263 K, Respectively

		fragment	D	D_c/D_a	r_H	r_H^{corr}	D	D_c/D_a	r_H	r_H^{corr}
					2 mM, 299 K					
			PF_6				BArF			
1. **3a**[b]		cation	13.02	0.96	4.1	5.0	12.32	1.45	4.3	5.2
		anion	13.54		3.9	4.9	8.48		6.2	6.8
2. **3b**		cation	12.58	0.93	4.2	5.1				
		anion	13.50		3.9	4.9				
3. **3g**		cation	10.84	0.86	4.9	5.6	10.40	1.24	5.1	5.8
		anion	12.63		4.2	5.1	8.40		6.3	6.8
4. **3h**		cation	10.73	0.84	4.9	5.7	9.94	1.19	5.3	6.0
		anion	12.79		4.1	5.1	8.35		6.3	6.9
5. **4e**		cation	10.33	0.79	5.1	5.8				
		anion	13.06		4.1	5.0				
6. **4g**		cation	10.13	0.78	5.2	5.9	9.45	1.13	5.6	6.2
		anion	12.98		4.1	5.0	8.35		6.3	6.9
7. **4h**		cation	9.49	0.73	5.6	6.2	8.92	1.08	5.9	6.5
		anion	12.95		4.1	5.0	8.25		6.4	7.0
					2 mM, 299 K, BPh_4					
8. **3a**		cation	12.32	1.18	4.3	5.2				
		anion	10.40		5.1	5.8				
9. **3b**		cation	11.68	1.17	4.5	5.3				
		anion	10.00		5.3	6.0				
10. **3c**		cation	12.24	1.21	4.3	5.2				
		anion	10.08		5.2	5.9				
					10 mM, 299 K					
11. **3a**	BPh_4	cation	10.84	1.12	4.9	5.6				
		anion	9.65		5.5	6.1				
12. **3a**	PF_6	cation	12.65	0.95	4.2	5.1				
		anion	13.32		4.0	4.9				
13. **3c**	BPh_4	cation	11.22	1.13	4.7	5.5				
		anion	9.89		5.4	6.0				
					10 mM, 263 K					
					PF_6				BArF	
14. **3a**		cation	7.40	0.92	4.4	5.2	6.99	1.37	4.6	5.4
		anion	8.08		4.0	4.9	5.12		6.3	6.8
15. **3b**		cation	7.37	0.95	4.4	5.2				
		anion	7.78		4.1	5.1				
16. **3h**		cation	5.82	0.84	5.5	6.2	5.72	1.19	5.6	6.3
		anion	6.95		4.6	5.4	4.81		6.7	7.2
17. **4e**		cation	5.94	0.82	5.4	6.1				
		anion	7.22		4.5	5.3				
18. **4g**		cation	5.70	0.80	5.6	6.3	4.77	1.07	6.8	7.3
		anion	7.16		4.5	5.3	4.44		7.3	7.4
19. **4h**		cation	5.39	0.86	6.0	6.6	5.04	0.92	6.4	6.9
		anion	6.24		5.2	5.9	5.47		5.9	6.5
					10 mM, 263 K, BPh_4					
20. **3a**		cation	6.09	1.14	5.3	6.0				
		anion	5.34		6.0	6.5				
21. **3c**		cation	6.34	1.19	5.1	5.8				
		anion	5.34		6.0	6.6				
22. **3d**		cation	5.60	1.02	5.8	6.4				
		anion	5.50		5.9	6.5				
23. **3e**		cation	5.72	1.08	5.6	6.3				
		anion	5.32		6.1	6.6				
24. **3e**		cation	5.35	1.05	6.0	6.6				
		anion	5.03		6.1	6.9				
25. **3f**		cation	5.65	1.04	5.7	6.3				
		anion	5.42		5.9	6.5				
26. **3g**		cation	5.38	1.06	6.0	6.6				
		anion	5.09		6.3	6.9				
27. **3h**		cation	5.38	1.03	6.0	6.6				
		anion	5.23		6.2	6.7				
28. **4e**		cation	5.33	1.01	6.0	6.6				
		anion	5.28		6.1	6.7				
29. **4g**		cation	5.12	0.99	6.3	6.8				
		anion	5.16		6.2	6.8				
30. **4h**		cation	5.45	1.02	5.9	6.5				
		anion	5.32		6.1	6.6				

Table 3. Continued

			2 mM, 263 K			
31. **3a**	BPh_4	cation	6.89	1.06	4.7	5.5
		anion	6.53		4.9	5.7
32. **3a**	PF_6	cation	7.54	0.92	4.3	5.2
		anion	8.17		3.9	4.9
33. **3a**	BArF	cation	7.82	1.47	4.0	5.1
		anion	5.33		6.0	6.6
34. **3g**	BPh_4	cation	5.91	1.07	5.5	6.1
		anion	5.53		5.8	6.4
35. **3h**	BPh_4	cation	5.86	1.04	5.5	6.1
		anion	5.65		5.7	6.3
36. **4g**	BPh_4	cation	5.67	0.99	5.7	6.3
		anion	5.72		5.6	6.3
37. **4h**	BPh_4	cation	5.38	0.97	6.0	6.6
		anion	5.52		5.8	6.4

[a] r_H was calculated using the Stokes−Einstein relation; r_H^{corr} was calculated using a semiempirical estimation of c (one iteration step).[63] For the calculation of r_H, the viscosity of CH_2Cl_2 at 299 and 263 K was used, respectively ($\eta(299\,K)=0.46\times10^{-3}\,kg\,s^{-1}\,m^{-1}$, $\eta(263\,K)=0.60\times10^{-3}\,kg\,s^{-1}\,m^{-1}$). [b] D values for **3a**(PF_6) for the cation/anion in acetone-d_6 (15.64/24.80) and methanol-d_4 (10.88/15.96) solution.

Scheme 3

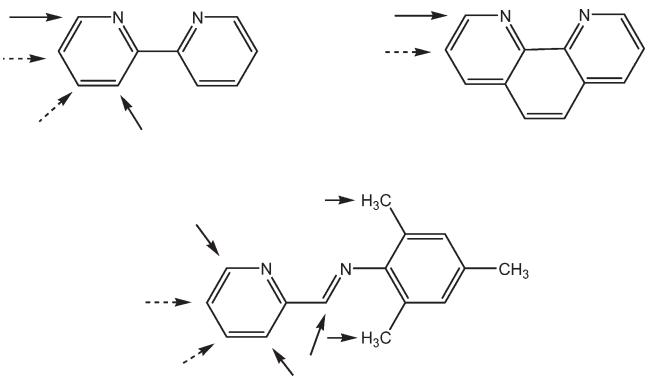

the N,N ligands change somewhat (see Scheme 3 for the most important in three examples). The solid arrows indicate the stronger, the dotted arrows the weaker interactions. The strong contacts are comparable to—or stronger than—those to the allyl ligand. The overall picture suggests that the PF_6^- anion sits above the N−Pd−N coordination plane, in a pseudocoordination position, and for asymmetric N,N ligands preferably on the side close to the pyridine. This latter point arises from (a) the stronger contact to the *syn* allyl proton as opposed to the *anti* allyl proton and (b) the fact that for the mesityl Schiff base shown, the anion seems to be placed somewhat closer to the pyridine moiety; that is, it is not in a classical fifth coordination position. Figure 4 shows the $^{19}F,^1H$ HOESY spectrum for salt **3g**(PF_6) at 263 K in CD_2Cl_2.

The selective cross-peaks indicate that the anion chooses to occupy a specific position, close to the Schiff base CH=N moiety and aryl proton H3′ (as indicated by the arrow), rather than move randomly around the exterior of the cation. This type of positional preference for the PF_6^- anion has been observed previously.[17]

For the 1,3-diphenyl allyl salts, **4**, a similar picture emerges with the PF_6^- anion occupying a pseudocoordination position. However, for these ligands, the anion resides on the side of the allyl ligand close to the two *anti* protons, but remote from the central allyl proton, in keeping with expected steric effects due to the two relatively large phenyl groups.

Turning to the BPh_4^- anion, Figure 5 shows a 2-D ROESY spectrum for salt **4e**(BPh_4) at 193 K in CD_2Cl_2. The three sets of BPh_4^- ^1H resonances (those located between δ 6.8 and 7.4 are indicated with a star) reveal cross-peaks to aryl protons H3′ and H3 as well as Schiff base proton H7′ among others. These data suggest that the BPh_4^- anion is positioned close to the bidentate ligand and that the solution structure is related to that of the solid state.

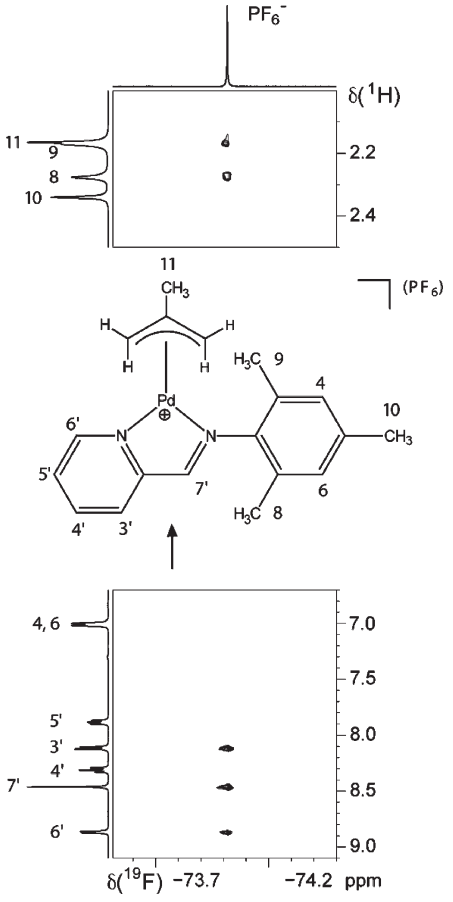

Figure 4. $^{19}F,^1H$ HOESY spectrum of **3g**(PF_6) at 263 K in CD_2Cl_2 (10 mM). Strong contacts to the α-diimine ligand protons 3′, 7′, 8, and 9 suggest an approach of the anion as indicated by the arrow. Interestingly, there is also a contact to proton 6′.

Summarizing, the Overhauser solution data support the idea that the BPh_4^- anion prefers to be located close to the chelating nitrogen ligands. Moreover, taken together with the NMR diffusion and crystallographic results, it is reasonable

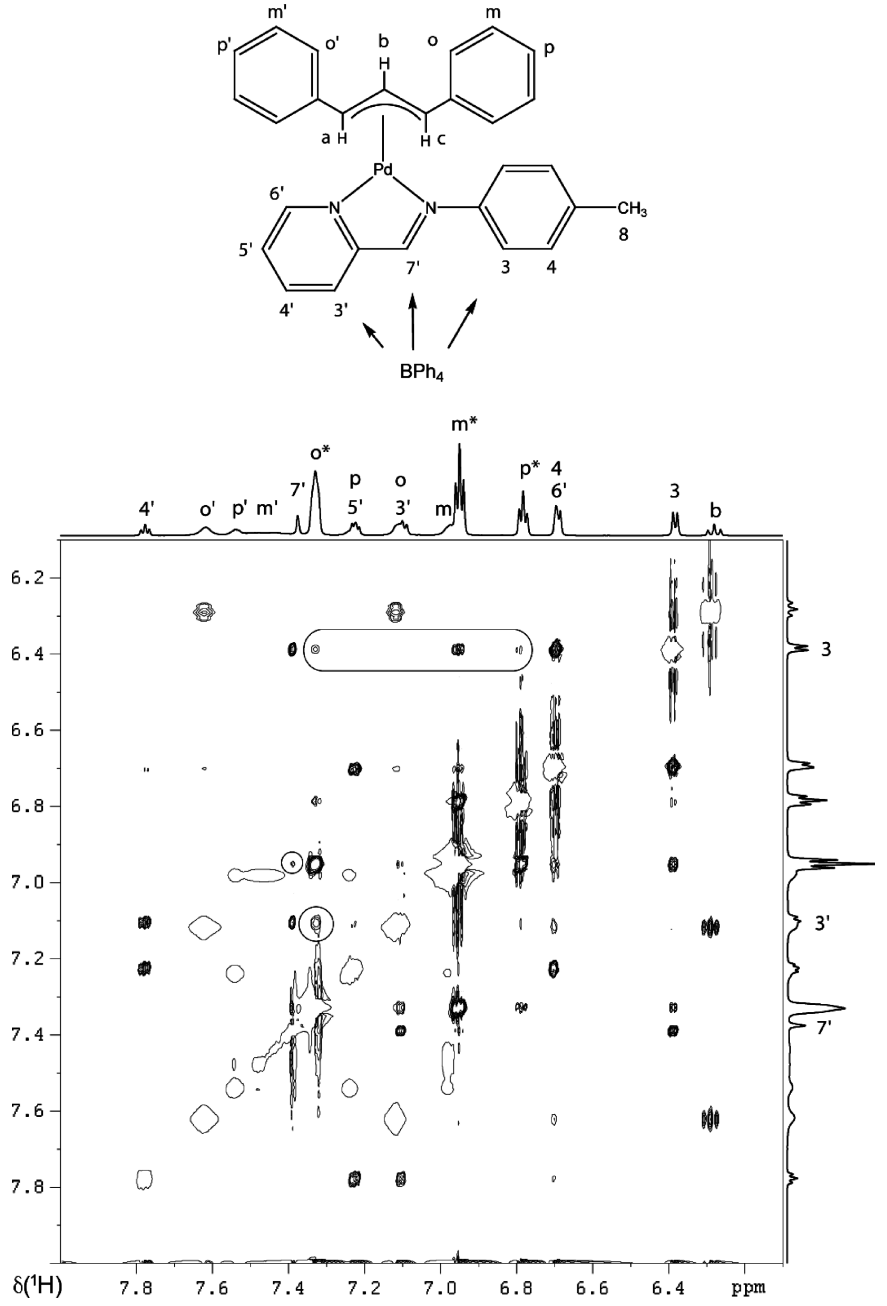

Figure 5. 700 MHz ^{1}H,^{1}H ROESY spectrum of **4e**(BPh_4) at 193 K in CD_2Cl_2 (10 mM). The anion shows contacts to protons 3, 3′, and 7′, respectively (see marks in the upper part of the spectrum; the resonances of the BPh_4 anion are labeled with an asterisk). Additionally, there are weak contacts to the allyl protons "a" and "c" (not shown). The single circle cross-peaks of the exchanging phenyl resonances are due to the apparent allyl rotation.

that (assuming an open coordination position becomes available) phenyl anion transfer will be a facile process.

Allyl Dynamics. Palladium allyl complexes are well known[31−37] to exhibit various dynamic processes including η^3 to η^1 isomerization, *syn*/*anti* H atom exchange (within the complexed allyl ligand), and "apparent" allyl rotation. According to the literature, these allyl isomerization processes may occur via different mechanisms and may be under

(31) Vrieze, K. Fluxional Allyl Complexes. In *Dynamic Nuclear Magnetic Resonance Spectroscopy*; Jackman, L. M.; Cotton, F. A., Eds.; Academic Press: New York, 1975; pp 441−483.

(32) Faller, J. W. In *Dynamic NMR Spectroscopy in Organometallic Chemistry, Comprehensive Organometallic Chemistry III*; Crabtree, R. H.; Mingos, D. M. P., Eds.; Elsevier: Oxford, 2006; pp 407−428.

(33) (a) Cesarotti, E.; Grassi, M.; Prati, L.; Demartin, F. *J. Organomet. Chem.* **1989**, *370*, 407–419. (b) Cesarotti, E.; Grassi, M.; Prati, L.; Demartin, F. *J. Chem. Soc., Dalton Trans.* **1991**, 2073.

(34) (a) Fernandez-Galan, R.; Jalon, F. A.; Manzano, B. R.; Rodriguez de la Fuente, J.; Vreahami, M.; Jedlicka, B.; Weissensteiner, W.; Jogl, G. *Organometallics* **1997**, *16*, 3758–3768. (b) Montoya, V.; Pons, J.; Garcia-Anton, J.; Solans, X.; Font-Bardia, M.; Ros, J. *Organometallics* **2007**, *26*, 3183–31990.

(35) (a) Wassenaar, J.; van Zutphen, S.; Mora, G.; Le Floch, P.; Siegler, M. A.; Spek, A. L.; Reek, J. N. H. *Organometallics* **2009**, *28*, 2724–2734. (b) Deng, W.; You, S.; Hou, X.; Dai, L.; Xia, W.; Sun, J. *J. Am. Chem. Soc.* **2001**, *123*, 6508–6519.

(36) Breutel, C.; Pregosin, P. S.; Salzmann, R.; Togni, A. *J. Am. Chem. Soc.* **1994**, *116*, 4067.

(37) Gogoll, A.; Ornebro, J.; Grennberg, H.; Bäckvall, J. E. *J. Am. Chem. Soc.* **1994**, *116*, 3631.

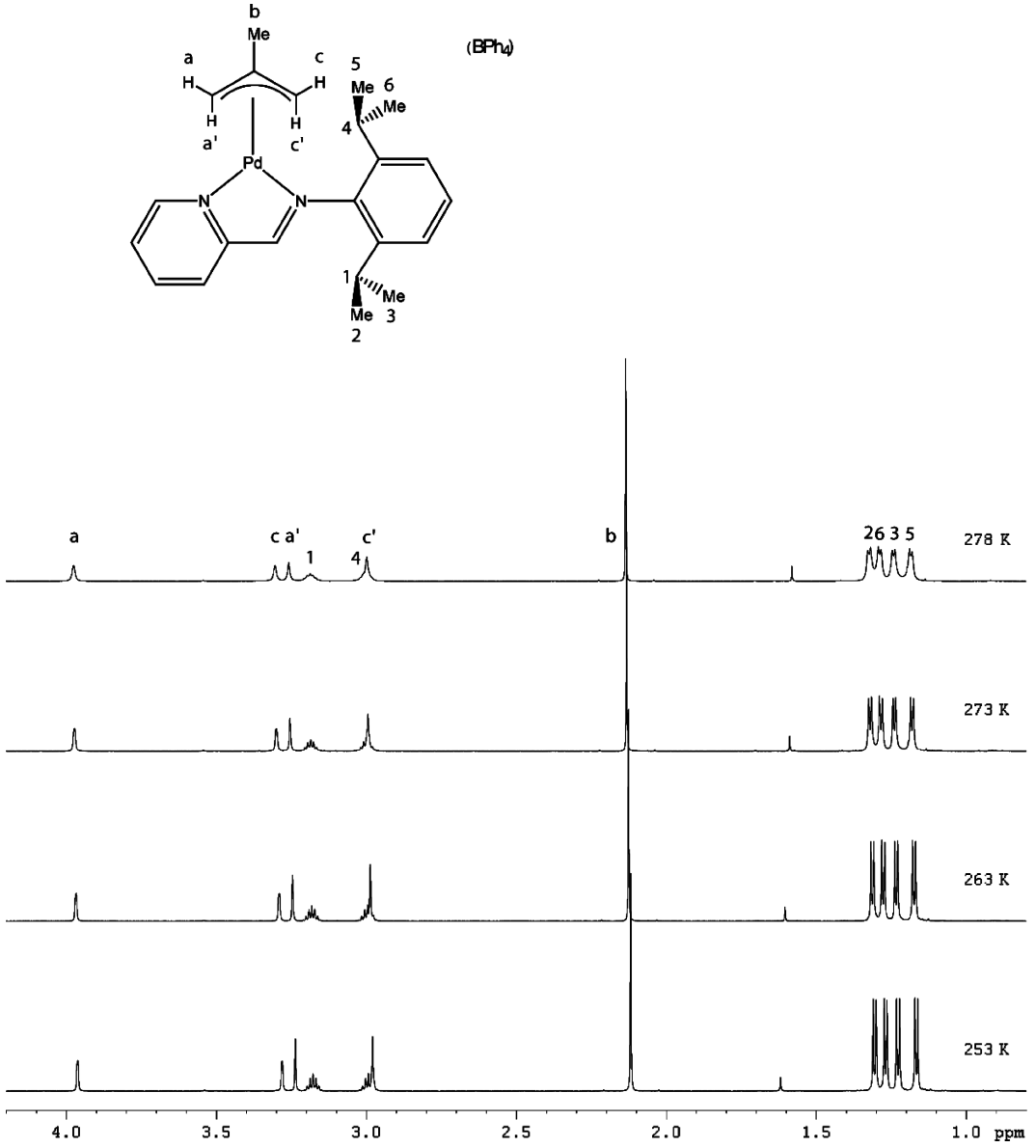

Figure 6. 700 MHz ^{1}H NMR variable-temperature spectra of **3h**(BPh_4) in CD_2Cl_2 (10 mM) from 253 to 278 K. The resonances of the allyl protons and the isopropyl groups have identical line broadening; that is, the dynamic processes responsible for their broadening are coupled.

either electronic or steric control.[36] Further, these dynamics may be associated with Pd−N bond breaking.[37] Given that "anion effects"[1] on various reactions are now fairly commonplace, we were curious as to the effect of our various anions on the dynamics associated with **3** and **4** and, specifically, if the BPh_4^- anion was in any way unusual.

Figures 6 and 7 show variable-temperature ^{1}H NMR studies for **3h** and **4h**, respectively, as BPh_4^- salts. Clearly, in both figures, lowering the temperature causes the various broad lines observed at ambient temperature to sharpen. In Figure 6 the four allyl and nonequivalent methine and methyl i-Pr resonances sharpen *at the same rate*. This is the case for most of our salts except for the three 1,3-diphenyl allyl analogues, **4h**(anion), and the behavior for one of these, **4h**(BPh_4), is illustrated in Figure 7. Here one sees that the two *anti* allyl protons, "a" and "c", found between $\delta = 4.7$ and $\delta = 5.1$, are quite sharp at 233 K, whereas the i-Pr resonances are still relatively broad. It would seem that for the cations **4h** we may have two different dynamic processes, perhaps because **4h** represents the most sterically crowded of all of our Pd cations.[38]

Figure 8 shows a section of the phase-sensitive 2-D ROESY for **3e**(BPh_4) at 213 K in CD_2Cl_2. The open cross-peaks have the same sign as the diagonal and arise from exchange. For both **3** and **4** an analysis of these 2-D data reveals selective *syn*/*syn*′ and *anti*/*anti*′ allyl proton exchange in all cases. We do *not* find *syn*/*anti* exchange.[39] There are many reports of this type of selective *syn*/*syn*′ and *anti*/*anti*′ exchange in Pd-allyl chemistry.[32,34b]

(38) The observed line broadening between two exchanging sites of equal population will depend on the difference in the frequencies, $\Delta\nu$, so that a direct comparison of, for example, the line shapes of two exchanging allyl protons with those for two exchanging methyl protons from the Schiff base is only valid if the $\Delta\nu$ values are identical.

(39) For examples of *syn*/*anti* exchange see: Kumar, P. G. A.; Dotta, P.; Hermatschweiler, R.; Pregosin, P. S.; Albinati, A.; Rizzato, S. *Organometallics* **2005**, *24*, 1306−1314, and Filipuzzi, S.; Pregosin, P. S.; Albinati, A.; Rizzato, S. *Organometallics* **2008**, *27*, 437−444. See also ref 32 for a review in which the subject is mentioned.

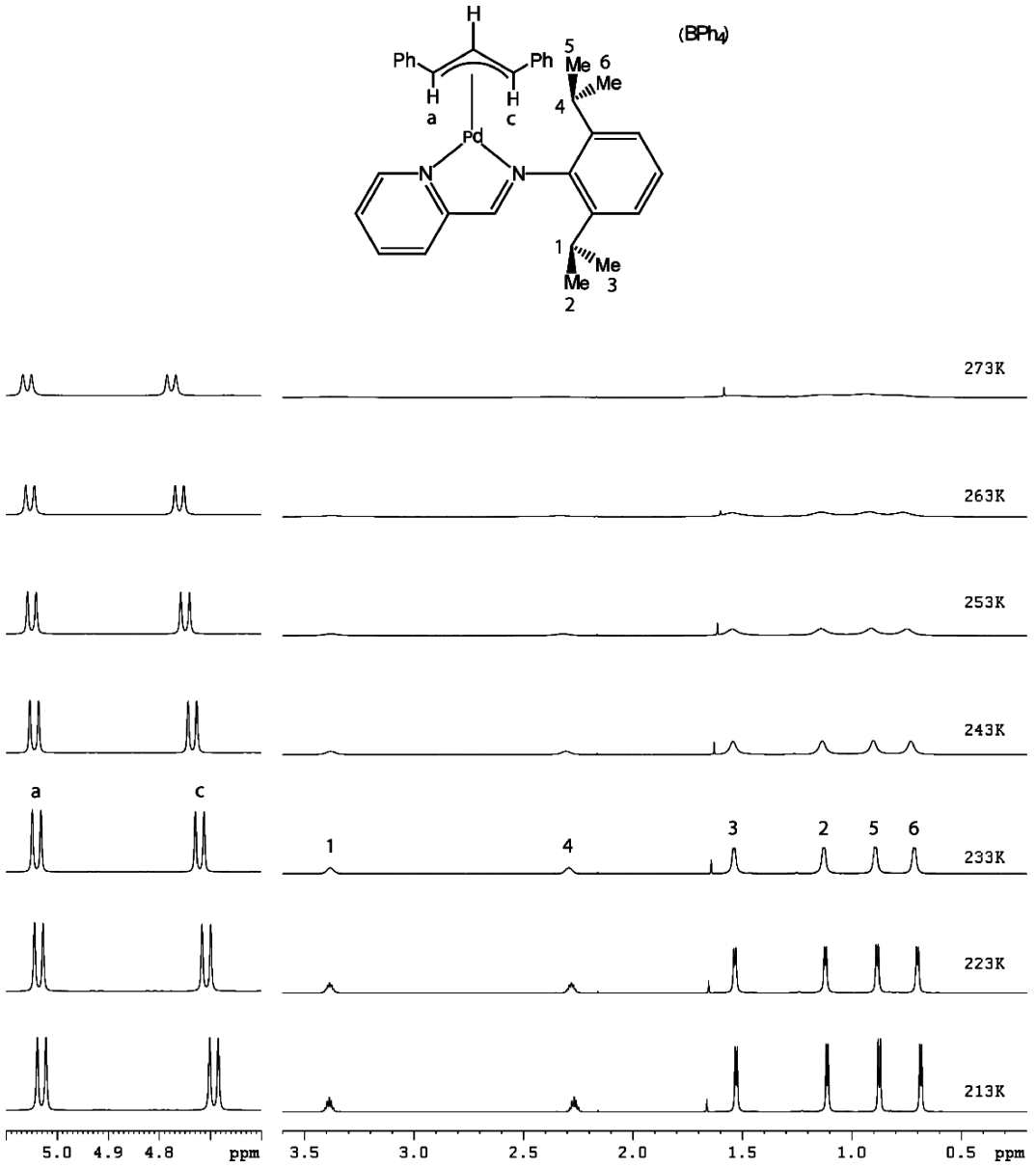

Figure 7. 700 MHz ^{1}H NMR variable-temperature spectra of **4h**(BPh_4) in CD_2Cl_2 (10 mM) from 213 to 273 K. The two *anti* allyl protons, "a" and "c", found between $\delta = 4.7$ and $\delta = 5.1$, are quite sharp at 233 K, whereas the i-Pr resonances are still relatively broad. It would seem that for the cations **4h** we may have two different dynamic processes.

Scheme 4

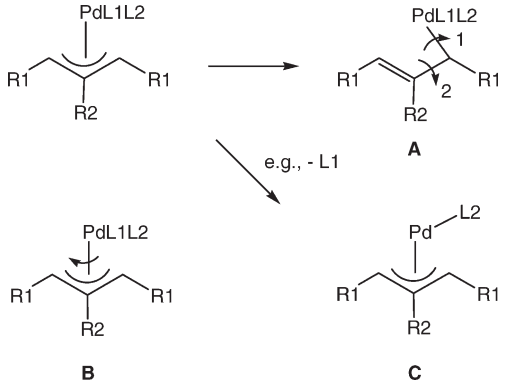

Using magnetization transfer methods we have determined the activation energies involved in these dynamics for the three anions BPh_4^-, PF_6^-, and $BArF^-$ of the catalytically more relevant 1,3-diphenyl cations **4g** and **4h** and show these results in Table 4. These values fall in the range ca. 10−13 kcal/mol and, assuming an error of ±1 kcal/mol, are not very different. The values for the salts **3** are on the order of 10 kcal/mol. We conclude that (consistent with the terminal allyl carbon ^{13}C chemical shifts of Table 1) the anion does not play an important role in these dynamics. Similar activation energies have been reported in earlier studies on Pd-allyl complexes.[34b]

The question of the mechanism of the dynamics remains open. An η^3 to η^1 isomerization to afford a three-coordinate species is possible and would result in *syn*/*anti* exchange if the η^1-complex undergoes a rotation around the C−C bond (arrow 2 of A in Scheme 4). However, this is not observed in our salts. Nevertheless, if the η^1-complex undergoes a rotation around the Pd−C bond (arrow 1 in Scheme 4)

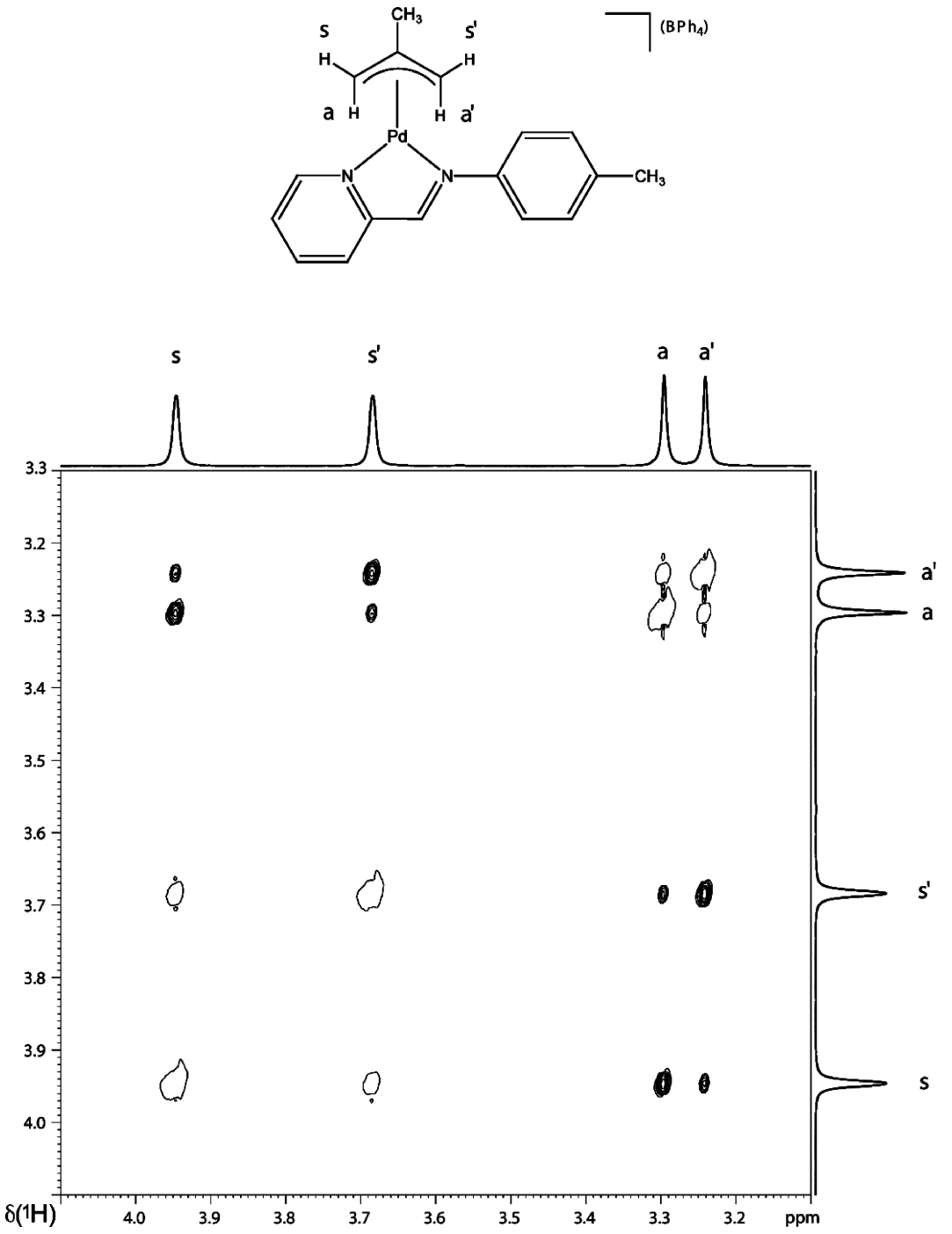

Figure 8. 700 MHz ^{1}H,^{1}H ROESY spectrum of **3e**(BPh_4) at 213 K in CD_2Cl_2 (10 mM). The single circle cross-peaks represent *syn*/*syn*′ and *anti*/*anti*′ proton exchange due to the apparent allyl rotation. Multi-circles show NOE contacts between corresponding *syn*/*anti* protons. Note the absence of *syn*/*anti* exchange.

and then isomerizes further;[39] this would shift the two R1 groups into different positions with respect to a salt having two different L-donor ligands. Alternatively, "apparent" allyl rotation as suggested by B in the scheme affords the same result. Continuing, an L dissociation[34,37] to afford a three-coordinate η^3-allyl species, such as C, or a possible five-coordinate complex (not shown) has also been discussed as a possible pathway for the observed *syn*/*syn*′ and *anti*/*anti*′ allyl isomerization.

In an effort to clarify the issue we have carried out experiments in which we have added from 1 to 10 equiv of CH_3CN to solutions of two of our salts, **3h**(PF_6) and **4h**-(PF_6). In this fashion we had hoped to find evidence for a possible η^1-complex such as **5**. For the 2-methyl allyl cation, **3h**(PF_6), we find no evidence for a new species; however, based on the new dependence of the line shapes, the isomerization rate *increases*. This rate increase is also observed in CD_3CN solution. For the larger 1,3-diphenyl allyl cation, **4h**(PF_6), we find *no change at all* upon addition of CH_3CN (see Figure S1). It would seem that an η^1-complex is not likely to be a major contributor; however, the addition of the nitrile seems to play some role for the salts of **3**, again

Table 4. Activation Energies for the Dynamics of the 1,3-Diphenyl Cations in 4g and 4h

		E_a/kcal mol^{-1}		
structure	anion	allyl		
4g	BPh_4	12.5	11.6	10 mM, 263 K
4g	PF_6	11.2	13.2	
4g	BArF	12.1	12.2	
4h	BPh_4	12.0	13.8	
4h	PF_6	10.2	10.4	
4h	BArF	9.7	11.2	

suggesting that the allyl structure is an important factor in the dynamics.

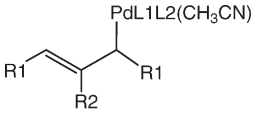

5

DFT Studies. The mechanism of the dynamic process described above for the allyl complexes **3g**, **4g**, and **4h** was investigated by means of DFT calculations.[40] The energy profile calculated for complex **3g** is represented in Figure 9. The corresponding profiles obtained for the complexes **4g** and **4h** are provided as Supporting Information.

In the reagent, **3g**, the metal coordination environment comprises the η^3-allyl ligand, formally occupying two adjacent coordination positions, and the two N atoms of the chelating ligand, occupying the remaining two positions of the square-planar geometry. In the first step of the calculated path, there is addition of one solvent molecule (via $\mathbf{TS1_{3g}}$) with formation of intermediate $\mathbf{I_{3g}}$. In this intermediate, $\mathbf{I_{3g}}$, the solvent molecule coordinates the metal through one Cl atom, and as a consequence, the Pd−N_{py} bond is broken. In $\mathbf{I_{3g}}$ the Pd−N_{py} distance is long (2.607 Å) and the corresponding Wiberg index (WI)[41] is small (0.059). These values differ considerably from those calculated for **3g**, where the Pd−N_{py} bond is well established: d = 2.136 Å and WI = 0.223. $\mathbf{I_{3g}}$ is a rather unstable intermediate, with an energy of 7.5 kcal/mol higher than the reactants, and, thus, should correspond to a short-lived species. The transition state associated with the first step, $\mathbf{TS1_{3g}}$, can be thought of as rather a late one, with both the formation of the Pd−Cl bond (d = 2.720 Å, WI = 0.110) and the breaking of the Pd−N_{py} interaction (d = 2.450 Å, WI = 0.085) well advanced. For comparison purposes, in intermediate $\mathbf{I_{3g}}$ the Pd−Cl distance is 2.588 Å and the Wiberg index is 0.150.

An important structural change, occurring along the first step, involves the relative position of the allyl ligand. In **3g**, the coordination plane of the complex is defined by the allyl ligand and the two N-atoms of the chelating ligand. The angle between the plane defined by the metal and the two terminal C_{allyl} atoms, and the N−Pd−N plane is $\alpha = 0°$. In the intermediate, $\mathbf{I_{3g}}$, the equivalent angle is $\alpha = 73°$, indicating a strong rotation of the allyl ligand with respect to the N−Pd−N plane. In $\mathbf{I_{3g}}$, the metal coordination sphere includes the Cl atom from CH_2Cl_2, the allyl ligand (η^3-coordinated), and the imine N atom. The angle between the plane defined by the two terminal C_{allyl} atoms and the Cl−Pd−N_{imine} plane in $\mathbf{I_{3g}}$ is $\beta = 6°$. In the calculated path, the solvent molecule, CH_2Cl_2, assists allyl rotation in complex **3g** by providing an intermediate ($\mathbf{I_{3g}}$) stabilized by a square-planar environment around the metal, in the middle of the rotation process. In the transition state $\mathbf{TS1_{3g}}$ the angle α, between the Pd-allyl plane and the Pd−N,N plane, is already 55°, indicating, once more, that $\mathbf{TS1_{3g}}$ is a late transition state.

In the second step depicted in Figure 9, from $\mathbf{I_{3g}}$ to $\mathbf{3g'}$, allyl rotation continues and the CH_2Cl_2 molecule is expelled from the coordination sphere. The product of this step, $\mathbf{3g'}$, represents the enantiomer of the initial complex, **3g**, and results from a 180° rotation of the allyl ligand. In the transition state associated with the second step, $\mathbf{TS2_{3g}}$, regeneration of the Pd−N_{py} bond is already evident, with a distance of 2.278 Å and an associated Wiberg index of 0.142.

The second half of the mechanism, represented on the right side of the profile in Figure 9, is completely equivalent to the first one, described above, and thus, no further discussion is warranted. It is the asymmetry present in the N,N ligand that causes the difference between the two halves of the profile. In the first half of the profile, the methyl substituent on allyl goes over the aryl group in the imine, while in the second half of the mechanism, as allyl rotation occurs the methyl substituent on allyl is brought to the side of the pyridine ring.

The rate-limiting step of the calculated mechanism is the second one, with an overall energy barrier of 13.1 kcal/mol. This value agrees reasonably well with the experimental activation energies (see Table 4) and is similar to the values calculated for complexes **4g** (12.7 kcal/mol) and **4h** (12.3 kcal/mol). The energy profiles obtained for these two species (see Supporting Information) are essentially equivalent to the one calculated for **3g**.

Alternative pathways involving allyl slippage from η^3 to η^1, induced for example by solvent coordination, were thoroughly tested. However, no such species could be optimized for complexes **4g** and **4h**, while in the case of **3g** the corresponding species, $[Pd(\eta^1\text{-allyl})(CH_2Cl_2)(N,N)]^+$, is 19 kcal/mol less stable than the reagents, thereby precluding its participation in the mechanism.

A rotation of the aryl substituent about the N_{imine}−C_{aryl} bond of the N,N ligand was also investigated by means of DFT calculations. This process was rather difficult to calculate due to the proximity between the aryl group and the allyl ligand in the complex. As a consequence, the resulting mechanisms involved strong disruption of the molecule structure and, thus, high energy barriers. The profile represented in Figure 10 was calculated for complex **3g** and corresponds to the most favorable mechanism obtained.

In the mechanism calculated for mesityl rotation in complex **3g** there is also participation of one CH_2Cl_2 molecule in a similar fashion to that described for allyl rotation. In the first step of the mechanism, from **3g** to $\mathbf{III_{3g}}$, there is coordination of the solvent molecule, with formation of one Pd−Cl bond, with simultaneous breaking of the Pd−N_{imine} bond. Cleavage of the Pd−N_{imine} bond proved essential in this mechanism, in order to increase the separation between the aryl group and the coordinated allyl ligand, thus reducing the unfavorable steric interactions.

However there is an important difference in intermediate $\mathbf{III_{3g}}$, relative to those present in the mechanism of allyl

(40) Parr, R. G.; Yang, W. *Density Functional Theory of Atoms and Molecules*; Oxford University Press: New York, 1989.

(41) (a) Wiberg, K. B. *Tetrahedron* **1968**, *24*, 1083. (b) Wiberg indices are electronic parameters related to the electron density between atoms. They can be obtained from a natural population analysis and provide an indication of the bond strength.

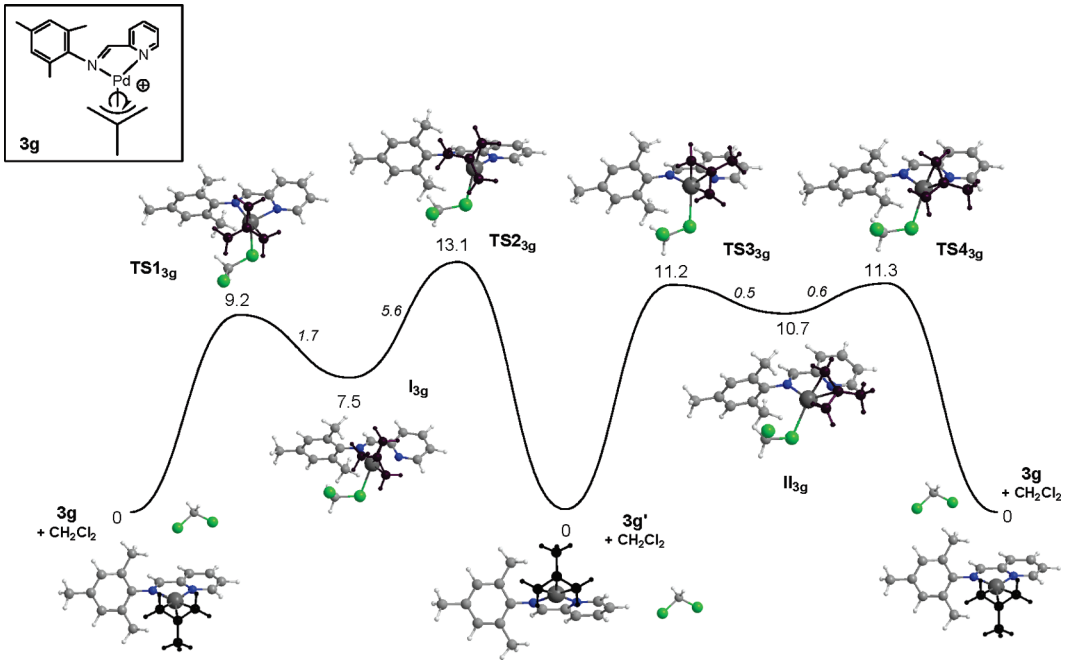

Figure 9. Energy profile calculated for the rotation of the 2-methyl allyl ligand in complex **3g**, with participation of one molecule of CH_2Cl_2. The minima and the transition states were optimized (PBE1PBE/VDZP), and the structures obtained are indicated next to their respective energies. The energy values (kcal/mol) are with respect to the reactants (**3g** plus one molecule of CH_2Cl_2, lower left in the figure), and the values in italics represent energy barriers. The allyl ligand is shown with darker circles, the chelate ligand is shown in gray, and the chloride atoms in CH_2Cl_2 are shown in green.

rotation, $\mathbf{I_{3g}}$ and $\mathbf{II_{3g}}$. In the mechanism of allyl rotation cleavage of the Pd−N_{py} bond followed solvent coordination with the N,N ligand maintaining a *cisoid* conformation of the central NCCN frame; that is, in the corresponding intermediates, $\mathbf{I_{3g}}$ and $\mathbf{II_{3g}}$, both N atoms were on the same side, pointing to the metal. Equivalent intermediates, with both N atoms pointing toward the metal, but with cleavage of the Pd−N_{imine} bond (while maintaining the Pd−N_{py} bond) could not be optimized for any of the complexes investigated, **3g**, **4g**, and **4h**. All attempts made for the optimization of such species resulted in CH_2Cl_2 loss and regeneration of the initial complex.

The only way that an intermediate with a dissociated Pd−N_{imine} bond could be obtained was through the rotation of the central NC−CN frame of the N,N ligand, and this is shown in the first step of the calculated mechanism, represented in Figure 10. In intermediate $\mathbf{III_{3g}}$, the NCCN dihedral angle is 176°, indicating that the two N atoms are on opposite sides of the N,N ligand: the N atom of the pyridine ring is coordinated to Pd, while the imine N atom points away from the metal. In the transition state associated with the first step, $\mathbf{TS5_{3g}}$, the NCCN dihedral angle (84°) is intermediate between the one present in $\mathbf{III_{3g}}$ and that observed in the reactant, **3g** (2°). Once the Pd−N_{imine} is broken in $\mathbf{III_{3g}}$, the rotation of the aryl group proceeds smoothly along two comparatively small barriers, $\mathbf{TS6_{3g}}$ and $\mathbf{TS7_{3g}}$. Each of these barriers corresponds to the passage of the 2,6-substituents in the ring (methyl groups in the case of mesityl, in complex **3g**) over each of the other ligands attached to the metal. Thus, in the first barrier ($\mathbf{TS6_{3g}}$) the mesityl ring goes over the solvent molecule (CH_2Cl_2), while in the second transition state ($\mathbf{TS7_{3g}}$) the aryl ring crosses the η^3-allyl ligand. Overcoming the two previous barriers corresponds to a complete revolution of the aryl ring (360°), and thus, $\mathbf{III_{3g}}$ is regenerated. Complex **3g** is obtained via a step equivalent to the first one, but going in the reverse sense: from $\mathbf{III_{3g}}$ to **3g**, with restoration of the Pd−N_{imine} bond and loss of CH_2Cl_2.

The rate-limiting steps of the entire process are the breaking and the formation of the Pd−N_{imine} bond, that is, the first and the last steps in the calculated mechanism. The activation energy calculated (21.1 kcal/mol) indicates that this mechanism is considerably less favorable than the one described above for allyl rotation. This same conclusion holds for complexes **4g** and **4h**, where the overall activation energy values calculated for aryl rotation were 17.9 and 20.5 kcal/mol, respectively. The corresponding mechanisms are equivalent to the one obtained for **3g**, and the energy profiles are presented as Supporting Information.

Conclusions

The diffusion NMR data reveal that the BPh_4^- salts do show a very substantial amount of ion pairing in dichloromethane solution, in keeping with Crociani's original suggestion. Both the solution Overhauser studies and the X-ray results are consistent with a BPh_4^- position that brings one or more phenyl groups very close to the N,N-chelate, and this would facilitate phenyl transfer. Despite this, and the observed local anisotropic effects that result in a low-frequency shift of several of the chelate ^{1}H resonances, there is little or no effect of this anion on the ^{13}C chemical shifts of these complexed allyl ligands.

The observed allyl and ligand dynamics fall under the general heading of "apparent rotation". We do not find any *syn*/*anti* isomerism. Although there are several mechanistic possibilities to account for this, the DFT calculations suggest that this isomerization process in **3** and **4** is solvent assisted and proceeds with Pd−N_{pyr} bond breaking. Both the experimental and calculated activation energies are in good agree-

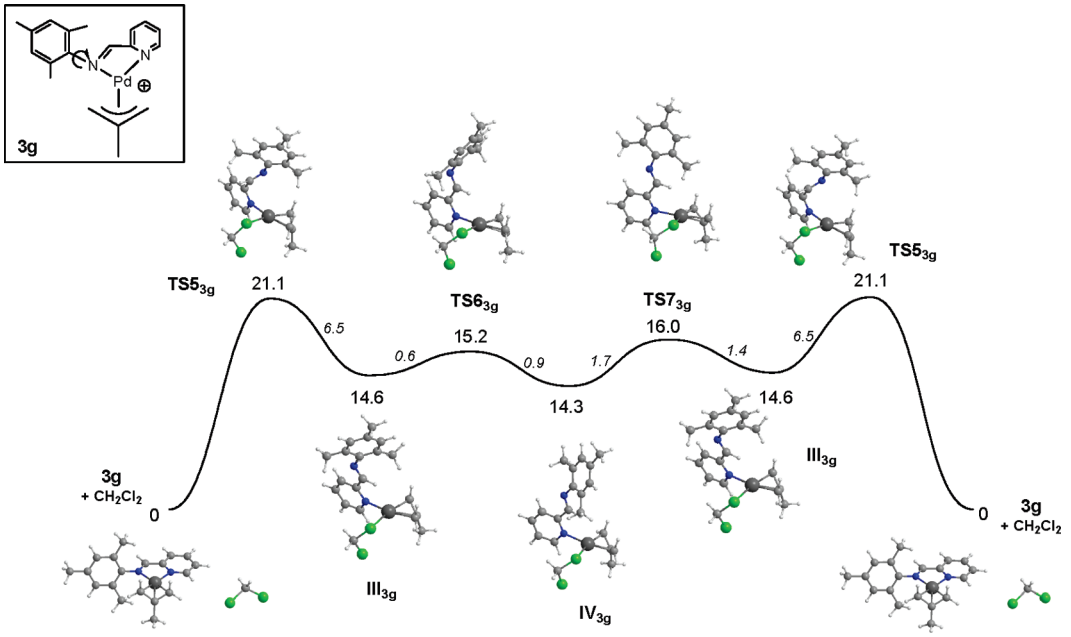

Figure 10. Energy profile calculated for the rotation of the mesityl group around the C−N_{imine} bond, in complex **3g**, with participation of one molecule of CH_2Cl_2. The minima and the transition states were optimized (PBE1PBE/VDZP), and the structures obtained are indicated next to their respective energies. The energy values (kcal/mol) are referred to the reactants (**3g** plus one molecule of CH_2Cl_2), and the values in italics represent energy barriers.

ment, and we do not find a significant effect of the BPh_4^- anion on these dynamics. On the basis of the calculations, the bulky substituents in the *ortho* positions of the Schiff base prevent rotation about the N−C bond so that the two nonequivalent methyl (or isopropyl) groups exchange only when the apparent allyl rotation occurs.

Experimental Section

The reactions were carried out with magnetic stirring and without special precautions against light or atmospheric moisture and oxygen, unless otherwise stated. Solvents were dried and distilled following standard procedures and stored under N_2. Deuterated dichloromethane was distilled over CaH_2 and degassed using two freeze−pump−thaw cycles and stored under N_2. All commercially available starting materials were purchased from commercial sources and used as received unless otherwise stated. NMR spectra were recorded with Bruker Avance 400 and 700 MHz spectrometers. Elemental analyses and mass spectroscopic studies were performed at ETHZ.

Computational Details. All calculations were performed using the GAUSSIAN 03 software package[42] and the PBE1PBE functional, without symmetry constraints. That functional uses a hybrid generalized gradient approximation (GGA), including 25% mixture of Hartree−Fock[43] exchange with DFT[40] exchange−correlation, given by the Perdew, Burke, and Ernzerhof functional (PBE).[44] The optimized geometries were obtained with a VDZP basis set (basis b1) consisting of the LanL2DZ basis set[45] augmented with an f-polarization function,[46] for Pd, and a standard 6-31G(d,p)[47] for the remaining elements. Transition-state optimizations were performed with the synchronous transit-guided quasi-Newton method (STQN) developed by Schlegel et al.[48] Frequency calculations were performed to confirm the nature of the stationary points, yielding one imaginary frequency for the transition states and none for the minima. Each transition state was further confirmed by following its vibrational mode downhill on both sides and obtaining

(42) Frisch, M. J.; Trucks, G. W.; Schlegel, H. B.; Scuseria, G. E.; Robb, M. A.; Cheeseman, J. R.; Montgomery, J. A., Jr.; Vreven, T.; Kudin, K. N.; Burant, J. C.; Millam, J. M.; Iyengar, S. S.; Tomasi, J.; Barone, V.; Mennucci, B.; Cossi, M.; Scalmani, G.; Rega, N.; Petersson, G. A.; Nakatsuji, H.; Hada, M.; Ehara, M.; Toyota, K.; Fukuda, R.; Hasegawa, J.; Ishida, M.; Nakajima, T.; Honda, Y.; Kitao, O.; Nakai, H.; Klene, M.; Li, X.; Knox, J. E.; Hratchian, H. P.; Cross, J. B.; Adamo, C.; Jaramillo, J.; Gomperts, R.; Stratmann, R. E.; Yazyev, O.; Austin, A. J.; Cammi, R.; Pomelli, C.; Ochterski, J. W.; Ayala, P. Y.; Morokuma, K.; Voth, G. A.; Salvador, P.; Dannenberg, J. J.; Zakrzewski, V. G.; Dapprich, S.; Daniels, A. D.; Strain, M. C.; Farkas, O.; Malick, D. K.; Rabuck, A. D.; Raghavachari, K.; Foresman, J. B.; Ortiz, J. V.; Cui, Q.; Baboul, A. G.; Clifford, S.; Cioslowski, J.; Stefanov, B. B.; Liu, G.; Liashenko, A.; Piskorz, P.; Komaromi, I.; Martin, R. L.; Fox, D. J.; Keith, T.; Al-Laham, M. A.; Peng, C. Y.; Nanayakkara, A.; Challacombe, M.; Gill, P. M. W.; Johnson, B.; Chen, W.; Wong, M. W.; Gonzalez, C.; Pople, J. A.*Gaussian 03*, Revision C.02; Gaussian, Inc.: Wallingford, CT, 2004.

(43) Hehre, W. J.; Radom, L.; Schleyer, P. v. R.; Pople, J. A. *Ab Initio Molecular Orbital Theory*; John Wiley & Sons: New York, 1986.

(44) (a) Perdew, J. P.; Burke, K.; Ernzerhof, M. *Phys. Rev. Lett.* **1997**, *78*, 1396. (b) Perdew, J. P. *Phys. Rev. B* **1986**, *33*, 8822.

(45) (a) Dunning, T. H., Jr.; Hay, P. J. *Modern Theoretical Chemistry*; Schaefer, H. F., III, Ed.; Plenum: New York, 1976; Vol. *3*, p 1. (b) Hay, P. J.; Wadt, W. R. *J. Chem. Phys.* **1985**, *82*, 270. (c) Wadt, W. R.; Hay, P. J. *J. Chem. Phys.* **1985**, *82*, 284. (d) Hay, P. J.; Wadt, W. R. *J. Chem. Phys.* **1985**, *82*, 2299.

(46) Ehlers, A. W.; Böhme, M.; Dapprich, S.; Gobbi, A.; Höllwarth, A.; Jonas, V.; Köhler, K. F.; Stegmann, R.; Veldkamp, A.; Frenking, G. *Chem. Phys. Lett.* **1993**, *208*, 111.

(47) (a) Ditchfield, R.; Hehre, W. J.; Pople, J. A. *J. Chem. Phys.* **1971**, *54*, 724. (b) Hehre, W. J.; Ditchfield, R.; Pople, J. A. *J. Chem. Phys.* **1972**, *56*, 2257. (c) Hariharan, P. C.; Pople, J. A. *Mol. Phys.* **1974**, *27*, 209. (d) Gordon, M. S. *Chem. Phys. Lett.* **1980**, *76*, 163. (e) Hariharan, P. C.; Pople, J. A. *Theor. Chim. Acta* **1973**, *28*, 213.

(48) (a) Peng, C.; Ayala, P. Y.; Schlegel, H. B.; Frisch, M. J. *J. Comput. Chem.* **1996**, *17*, 49. (b) Peng, C.; Schlegel, H. B. *Isr. J. Chem.* **1994**, *33*, 449.

(49) (a) Carpenter, J. E.; Weinhold, F. *J. Mol. Struct. (THEOCHEM)* **1988**, *169*, 41. (b) Carpenter, J. E. Ph.D. thesis, University of Wisconsin, Madison, WI, 1987. (c) Foster, J. P.; Weinhold, F. *J. Am. Chem. Soc.* **1980**, *102*, 7211. (d) Reed, A. E.; Weinhold, F. *J. Chem. Phys.* **1983**, *78*, 4066. (e) Reed, A. E.; Weinhold, F. *J. Chem. Phys.* **1983**, *78*, 1736. (f) Reed, A. E.; Weinstock, R. B.; Weinhold, F. *J. Chem. Phys.* **1985**, *83*, 735. (g) Reed, A. E.; Curtiss, L. A.; Weinhold, F. *Chem. Rev.* **1988**, *88*, 899. (h) Weinhold, F.; Carpenter, J. E. *The Structure of Small Molecules and Ions*; Plenum: New York, 1988; p 227.

the minima presented on the energy profiles. A natural population analysis (NPA)[49] and the resulting Wiberg indices[41] were used to study the electronic structure and bonding of the optimized species.

The energy profiles reported result from single-point energy calculations using a VTZP basis set (basis b2), and the geometries were optimized at the PBE1PBE/b1 level. Basis b2 consisted of a standard 3-21G[50] with an added f-polarization function[46] for Pd and standard 6-311++G(d,p)[51] for the remaining elements. Solvent (dichloromethane) effects were considered in the PBE1PBE/b2//PBE1PBE/b1 energy calculations using the polarizable continuum model (PCM) initially devised by Tomasi and co-workers[52] as implemented in Gaussian 03,[53] and thus, the energy values can be taken as free energy.[54] The molecular cavity was based on the united atom topological model applied on UAHF radii, optimized for the HF/6-31G(d) level.

Crystallography. Crystals of **3a**(BPh_4), **3b**(BPh_4), **3f**(BPh_4), **3h**(PF_6), and **4g**(PF_6) were mounted on a Bruker APEX II CCD diffractometer for the unit cell and space group determinations and for the data collections. For the low-temperature data collections crystals were cooled using a cold nitrogen stream. Selected crystallographic and other relevant data are listed in Table 2 and in the Supporting Information.

Data were corrected for Lorentz and polarization factors with the data reduction software SAINT[55] and empirically for absorption using the SADABS program.[56]

The structures were solved by direct and Fourier methods and refined by full matrix least-squares[57] (the function minimized being $\sum[w(|F_o|^2 - 1/k|F_c^2|)^2]$). For all structures, no extinction correction was deemed necessary. The scattering factors used, corrected for the real and imaginary parts of the anomalous dispersion, were taken from the literature.[58] All calculations and plotting were carried out by using the PC version of SHELX-97,[57] WINGX, ORTEP,[59] and Mercury programs[60]

Structural Study of 3a(BPh_4). The space group was unambiguously determined from the systematic absences, while the cell constants (at 150 K) were refined by least-squares, at the end of the data collection, using reflections up to $\theta_{max} \leq 22.2°$. The least-squares refinement was carried out using anisotropic displacement parameters for all non-hydrogen atoms. The H atoms of the cation were located from difference Fourier maps and their coordinates was refined with isotropic temperature factors fixed at $B(H) = 1.2B(C_{bonded})$. The contribution of the remaining hydrogens, in their calculated positions (C−H = 0.96 Å, $B(H) = 1.2B(C_{bonded})$ (Å^2)), was included in the refinement using a riding model.

Structural Study of 3b(BPh_4). The space group was assumed to be $P\bar{1}$ (no. 2), and the centrosymmetric choice was confirmed by the successful refinement. The cell constants at 150 K were obtained by least-squares fit, at the end of the data collection, using reflections up to $\theta_{max} \leq 20.9°$. The least-squares refinement was carried out using anisotropic displacement parameters for all non-hydrogen atoms, while the H atoms were included in the refinement as described above.

Structural Study of 3f(BPh_4). The space group was determined from the systematic absences, and the cell constants were refined by least-squares, at the end of the room-temperature data collection, using reflections up to $\theta_{max} \leq 23.6°$.

The least-squares refinement was carried out using anisotropic displacement parameters for all non-hydrogen atoms. The contribution of the hydrogen atoms, in their calculated positions (C−H = 0.96 Å, $B(H) = aB(C_{bonded})$ (Å^2) with $a = 1.5$ for the hydrogen atoms of the methyl groups, 1.2 for the others), was included in the refinement using a riding model.

Structural Study of 3h(PF_6). Space group and cell constants were determined at 150 K. The values of the cell parameters were refined at the end of the data collection using reflections up to $\theta_{max} \leq 29.2°$. In the Fourier difference maps two different orientations for one of the two isopropyl groups (that bonded to C3) were clearly shown; therefore, two carbon atoms were used to model this disorder and refined isotropically (site occupancy factor 0.5). The least-squares refinement was carried out using anisotropic displacement parameters for all non-hydrogen atoms not affected by disorder.

The H atoms of the allyl ligand were found from difference Fourier maps and their coordination was refined with isotropic temperature factors kept fixed at $B(H) = 1.2B(C_{bonded})$; the contribution of the remaining hydrogen atoms, in their calculated positions (C−H = 0.96 Å, $B(H) = aB(C_{bonded})$ (Å^2) with a = 1.5 for the hydrogen atoms of the methyl groups, 1.2 for the others), was included in the refinement using a riding model. Refining the Flack parameter tested the handedness of the structure.[61]

Structural Study of 4g[PF_6]. Unfortunately only low-quality, poorly diffracting crystals (see below) could be found. The space group was assumed to be $P\bar{1}$ (no. 2), and the centrosymmetric choice was later confirmed by the successful refinement. The cell constants were refined by least-squares, at the end of the RT data collection, using reflections up to $\theta_{max} \leq 23.5°$. There are two independent molecules in the asymmetric unit; however, there are no chemically significant differences in the immediate coordination spheres of the Pd atoms or in the bond distances and angles of both the anions and the cations.

The PF_6^- counterions are very disordered, as can be judged from the large ADPs. One of the PF_6^- moieties showed clearly, in the Fourier difference maps, positional disorder of the four equatorial fluorine atoms that could be modeled assuming three different orientations for each of the F atoms; the disordered atoms were refined isotropically (leading to occupancy factors of 0.5, 0.3, and 0.2, respectively). No reasonable model could be found for the other counterion, where rotational disorder, unhindered by any short contact with the cation, is present. The ADPs of the F atoms, allowed to refine anisotropically, show the situation clearly. Toward the end of the refinement a Fourier difference map revealed a disordered clathrated diethyl ether molecule that was included in the refinement, using isotropic temperature factors and a slack-constraint for the

(50) (a) Binkley, J. S.; Pople, J. A.; Hehre, W. J. *J. Am. Chem. Soc.* **1980**, *102*, 939. (b) Gordon, M. S.; Binkley, J. S.; Pople, J. A.; Pietro, W. J.; Hehre, W. J. *J. Am. Chem. Soc.* **1982**, *10*, 2797. (c) Pietro, W. J.; Francl, M. M.; Hehre, W. J.; Defrees, D. J.; Pople, J. A.; Binkley, J. S. *J. Am. Chem. Soc.* **1982**, *104*, 5039. (d) Dobbs, K. D.; Hehre, W. J. *J. Comput. Chem.* **1986**, *7*, 359. (e) Dobbs, K. D.; Hehre, W. J. *J. Comput. Chem.* **1987**, *8*, 861. (f) Dobbs, K. D.; Hehre, W. J. *J. Comput. Chem.* **1987**, *8*, 880.

(51) (a) McClean, A. D.; Chandler, G. S. *J. Chem. Phys.* **1980**, *72*, 5639. (b) Krishnan, R.; Binkley, J. S.; Seeger, R.; Pople, J. A. *J. Chem. Phys.* **1980**, *72*, 650. (c) Wachters, A. J. H. *J. Chem. Phys.* **1970**, *52*, 1033. (d) Hay, P. J. *J. Chem. Phys.* **1977**, *66*, 4377. (e) Raghavachari, K.; Trucks, G. W. *J. Chem. Phys.* **1989**, *91*, 1062. (f) Binning, R. C.; Curtiss, L. A. *J. Comput. Chem.* **1995**, *103*, 6104. (g) McGrath, M. P.; Radom, L. *J. Chem. Phys.* **1991**, *94*, 511.

(52) (a) Cancès, M. T.; Mennucci, B.; Tomasi, J. *J. Chem. Phys.* **1997**, *107*, 3032. (b) Cossi, M.; Barone, V.; Mennucci, B.; Tomasi, J. *Chem. Phys. Lett.* **1998**, *286*, 253. (c) Mennucci, B.; Tomasi, J. *J. Chem. Phys.* **1997**, *106*, 5151.

(53) Tomasi, J.; Mennucci, B.; Cammi, R. *Chem. Rev.* **2005**, *105*, 2999.

(54) Cossi, M.; Scalmani, G.; Rega, N.; Barone, V. *J. Chem. Phys.* **2002**, *117*, 43.

(55) BrukerAXS. *SAINT*, Integration Software; Bruker Analytical X-ray Systems: Madison, WI, 1995.

(56) Sheldrick, G. M. *SADABS, Program for Absorption Correction*; University of Göttingen: Göttingen, Germany, 1996.

(57) Sheldrick, G. M. *Acta Crystallogr.* **2008**, *A64*, 112.

(58) *International Tables for X-ray Crystallography*; Wilson, A. J. C., Ed.; Kluwer Academic Publisher: Dordrecht, The Netherlands, 1992; Vol. *C*.

(59) Farrugia, L .J. *J. Appl. Crystallogr.* **1997**, *30*, 565. Farrugia, L .J. *J. Appl. Crystallogr.* **1999**, *32*, 837.

(60) *Mercury* CSD 2.2 (Build RC5); The Cambridge Crystallographic Data Center: Cambridge, UK, 2009.

(61) Flack, H. D. *Acta Crystallogr.* **1983**, *A39*, 876.

C−C bond distances. The poor high-angle diffraction is a consequence of the disorder.

The least-squares refinement was carried out using anisotropic displacement parameters for all atoms not affected by disorder, while the contribution of the hydrogen atoms, in their calculated positions (C−H = 0.96 Å, B(H) = $aB(C_{bonded})$ (Å^2) with $a = 1.5$ for the hydrogen atoms of the methyl groups, 1.2 for the others), was included using a riding model.

NMR Measurements. All the PGSE diffusion measurements were performed using the standard stimulated echo pulse sequence on a 400 MHz Bruker Avance spectrometer equipped with a microprocessor-controlled gradient unit and an inverse multinuclear probe with an actively shielded Z-gradient coil. The shape of the gradient pulse was rectangular, its duration δ was 1.75 ms, and its strength varied automatically in the course of the experiments. The calibration of the gradients was carried out via a diffusion measurement of HDO in D_2O at ambient temperature. The data obtained were used to calculate the D values of the samples, according to the literature.[62]

PGSE Measurements at Ambient Temperature. Samples of 2 and 10 mM, respectively, were prepared in 0.5 mL of deuterated dichloromethane in a 5 mm diameter NMR tube. In the ^{1}H-PGSE experiments, Δ^{16} was set to 117.75 and 167.75 ms, respectively. The number of scans was 16 per increment with a recovery delay of 12 to 25 s. Typical experimental times were 2−6 h. For ^{19}F, Δ was set to 117.75 and 167.75 ms, respectively. Sixteen scans were taken with a recovery delay of 18 to 25 s and a total experimental time of ca. 2.5−6 h.

PGSE Measurements at 263 K. Samples of 2 and 10 mM, respectively, were prepared in 0.07 mL of deuterated dichloromethane. In order to overcome the convection problem in low-temperature PGSE diffusion measurements, a coaxial insert (with a diameter of 1.5 mm) inside a normal 5 mm NMR tube was employed as described earlier.[28]

In the ^{1}H-PGSE experiments, Δ^{16} was set to 117.75 and 167.75 ms, respectively. The number of scans varied between 24 and 64 scans per increment with a recovery delay of 12 to 25 s. Typical experimental times were 4−10 h. For ^{19}F, Δ was set to 117.75 and 167.75 ms, respectively; 24−64 scans were taken with a recovery delay of 18 to 25 s and a total experimental time of ca. 6−10 h.

All the spectra were acquired using 32K points and processed with a line broadening of 1 Hz (^{1}H) and 2 Hz (^{19}F). The slopes of the lines, m, were obtained by plotting their decrease in signal intensity versus G^2 using a standard linear regression algorithm. Normally, 14−20 points were used for regression analysis, and all of the data leading to the reported D values afforded lines whose correlation coefficients were >0.999. The gradient strength was incremented in 3−4% steps from 3 to 4% to 60−80%.

A measurement of ^{1}H and ^{19}F T_1 was carried out before each diffusion experiment, and the recovery delay set to 5 times T_1. We estimate the experimental error in D values at ±2%. The hydrodynamic radii, r_H, were estimated using the Stokes−Einstein equation ($c = 6$) or by introducing a semiempirical estimation of the c factor.[63]

The ^{19}F,^{1}H HOESY measurements were acquired using the standard four-pulse sequence[64] on a 400 MHz Bruker Avance spectrometer equipped with a doubly tuned (^{1}H, ^{19}F) TXI probe. A mixing time of 800 ms was used. The number of scans was 8−16 and the number of increments in the F1 dimension 512. The delay between the increments was set to 0.8 s. The concentration of the sample was 10 mM.

The ^{1}H,^{1}H ROESY measurements were acquired on a 400 and 700 MHz Bruker Avance spectrometer, respectively, both equipped with a multinuclear inverse probe. The concentration of the sample was 10 mM unless otherwise stated. A spin-lock pulse of 400 ms duration was used. The number of scans per increment was 32, and 1K experiments were acquired in the second dimension. The total experimental times were approximately 12 h.

Magnetization transfer experiments were performed by using the selective inversion-exchange/recovery monitoring scheme according to the literature.[65] For fitting the monitored data of the magnetization transfer experiments the CIFIT program package was used.[66]

Preparation of the α-Diimines. Bipy, phenanthroline, and TMEDA were purchased from commercial sources and used as received. The symmetric α-diimine **d**[67] and the pyridine-2-carbaldimines **e**,[68] **f**,[69] **g**,[70] and **h**[70] were prepared by published methods.

Preparation of [Pd(η^3-allyl)(N,N′)]X. The allylic chloro-bridged dimers[3] (allyl = 2-Me-C_3H_4, 1,3-diphenylallyl) were prepared by published methods. The mostly new cationic complexes **3a**, **3g**, **3h**, **4g**, **4h** (X) (X = BPh_4, PF_6, BArF), **3b**, **4e** (X = BPh_4, PF_6), and **3c**−**f** (X = BPh_4) were synthesized following a slightly modified literature procedure:[71] The suitable allylic chloro-bridged dimer (32 mg, 0.081 mmol) and the ligand (25 mg, 0.162 mmol) were mixed together in methanol (3 mL). After the solution was cooled to 0 °C, dropwise addition of the suitable sodium salt (54.7 mg, 0.162 mmol), dissolved in MeOH/H_2O (3 mL, 2:1 v/v), caused the immediate precipitation of a yellow solid, which was stirred for 5 min and filtered off. Repeated washings with H_2O and MeOH/H_2O (2:1, v/v) gave the pure product, which was dried in vacuo (40 mg, 78%).

[Pd(η^3-2-MeC_3H_4)(bipy)]BPh_4 (**3a**(BPh_4)),[72] [Pd(η^3-2-MeC_3H_4)-(py-2-CH=NC_6H_4OMe-4)]BPh_4 (**3f**(BPh_4)), and [Pd(η^3-2-MeC_3H_4)(-C(Me)=N NC_6H_4OMe-4)$_2$]BPh_4 (**3d**(BPh_4))[71] were described elsewhere some time ago.

^{1}H and ^{13}C NMR chemical shift data for the new salts can be found in Table S1 in the Supporting Information.

[Pd(η^3-2-MeC_3H_4)(bipy)]PF_6 (3a(PF_6)): white solid, yield 82%. Anal. Calcd for $C_{14}H_{15}F_6N_2PdP$: C, 36.34; H, 3.27; N, 6.05. Found: C, 36.43; H, 3.26; N, 5.94.

[Pd(η^3-2-MeC_3H_4)(bipy)]BArF (3a(BArF)): white solid, yield 81%. Anal. Calcd for $C_{46}H_{27}N_2BF_{24}Pd$: C, 46.79; H, 2.30; N, 2.37. Found: C, 46.76; H, 2.52; N, 2.33.

[Pd(η^3-2-MeC_3H_4)(phen)]PF_6 (3b(PF_6)): white solid, yield 76%. Anal. Calcd for $C_{16}H_{15}N_2F_6PPd$: C, 39.49; H, 3.11; N, 5.76. Found: C, 39.45; H, 3.13; N, 5.58.

[Pd(η^3-2-MeC_3H_4)(phen)]BPh_4 (3b(BPh_4)): white solid, yield 86%. Anal. Calcd for $C_{40}H_{35}N_2BPd$: C, 72.69; H, 5.34; N, 4.24. Found: C, 71.79; H, 5.41; N, 4.21.

[Pd(η^3-2-MeC_3H_4)(TMEDA)]BPh_4 (3c(BPh_4)): white solid, yield 60%. Anal. Calcd for $C_{34}H_{43}N_2BPd$: C, 68.41; H, 7.26; N, 4.69. Found: C, 68.32; H, 7.22; N, 4.63.

[Pd(η^3-2-MeC_3H_4)(py-2-CH=NC_6H_4Me-4)]BPh_4 (3e(BPh_4)): yellow solid, yield 74%. Anal. Calcd for $C_{41}H_{39}N_2BPd$: C, 72.74; H, 5.81; N, 4.14. Found: C, 72.27; H, 5.69; N, 3.96.

(62) Moreno, A.; Pregosin, P. S.; Veiros, L. E.; Albinati, A.; Rizzato, S. *Chem.−Eur. J.* **2009**, *15*, 6848–6862.
(63) (a) Gierer, A.; Wirtz, K. *Z. Naturforsch., A: Phys. Sci.* **1953**, *8* (9), 532–538. (b) Chen, H. C.; Chen, S. H. *J. Phys. Chem.* **1984**, *88*, 5118–5121.
(64) Rinaldi, P. L. *J. Am. Chem. Soc.* **1983**, *105*, 5167–5168.
(65) Led, J. J.; Gesmar, H. *J. Magn. Reson.* **1982**, *49*, 444–463.
(66) (a) The CIFIT program package was used for the simulations and data evaluation: Bain, A. D.; Cramer, J. A. *J. Magn. Reson.* **1996**, *118*, 21−27. (b) Muhandiramm, D. R.; McClung, R. E. D. *J. Magn. Reson.* **1987**, *71*, 187.
(67) Pramod, B.; Pansuriya, M. N. P. *Appl. Organomet. Chem.* **2007**, *21*, 739–749.
(68) Tanaka, K.; Shiraishi, R. *Green Chem.* **2000**, *2*, 272–273.
(69) Hartley, F. R.; Jones, S. R. *J. Organomet. Chem.* **1974**, *66*, 465–473.
(70) Diez, V.; Cuevas, J. V.; Garcia-Herbosa, G.; Aullon, G.; Charmant, J. P. H.; Carbayo, A.; Munoz, A. N. *Inorg. Chem.* **2007**, *46*, 568–577.
(71) Crociani, B.; di Bianca, F.; Giovenco, A.; Boschi, T. *Inorg. Chim. Acta* **1987**, *127*, 169–182.
(72) Ishii, Y.; Hasegawa, S.; Kimura, S.; Itoh, K. *J. Organomet. Chem.* **1974**, *73*, 411–418.

[Pd(η^3-2-MeC$_3$H$_4$)(py-2-CH=NMes)]PF$_6$ (3g(PF$_6$)): yellow solid, yield 53%. Anal. Calcd for $C_{19}H_{23}N_2F_6PPd$: C, 42.99; H, 4.37; N, 5.28. Found: C, 42.90; H, 4.33; N, 5.20.

[Pd(η^3-2-MeC$_3$H$_4$)(py-2-CH=NMes)]BPh$_4$ (3g(BPh$_4$)): yellow solid, yield 81%. Anal. Calcd for $C_{43}H_{43}N_2BPd$: C, 73.25; H, 6.15; N, 3.97. Found: C, 72.68; H, 6.38; N, 3.96.

[Pd(η^3-2-MeC$_3$H$_4$)(py-2-CH=NMes)]BArF (3g(BArF)): yellow solid, yield 84%. Anal. Calcd for $C_{51}H_{38}N_2BF_{24}Pd$: C, 48.92; H, 3.06; N, 2.24. Found: C, 49.14; H, 2.85; N, 2.21.

[Pd(η^3-2-MeC$_3$H$_4$)(py-2-CH=NC$_6$H$_4$(i-Pr)$_2$-2,6)]PF$_6$ (3h(PF$_6$)): yellow solid, yield 64%. Anal. Calcd for $C_{22}H_{29}N_2F_6PPd$: C, 46.13; H, 5.10; N, 4.89. Found: C, 46.33; H, 5.13; N, 4.83.

[Pd(η^3-2-MeC$_3$H$_4$)(py-2-CH=NC$_6$H$_4$(i-Pr)$_2$-2,6)]BPh$_4$ (3h(BPh$_4$)): yellow solid, yield 92%. Anal. Calcd for $C_{46}H_{49}N_2BPd$: C, 73.95; H, 6.61; N, 3.75. Found: C, 73.36; H, 6.91; N, 3.71.

[Pd(η^3-2-MeC$_3$H$_4$)(py-2-CH=NC$_6$H$_4$(i-Pr)$_2$-2,6)]BArF (3h(BArF)): yellow solid, yield 57%. Anal. Calcd for $C_{63}H_{47}N_2BF_{24}Pd$: C, 53.85; H, 3.37; N, 1.99. Found: C, 54.12; H, 3.18; N, 2.12.

[Pd(η^3-1,3-DiphenylC$_3$H$_3$)(py-2-CH=NC$_6$H$_4$Me-4)]PF$_6$ (4e(PF$_6$)): yellow solid, yield 65%. MALDI MS: 495.0 (M^+), 299.0 ($M^+ - \alpha$-diimine).

[Pd(η^3-1,3-DiphenylC$_3$H$_3$)(py-2-CH=NC$_6$H$_4$Me-4)]BPh$_4$ (4e(BPh$_4$)): yellow solid, yield 81%. Anal. Calcd for $C_{52}H_{45}N_2BPd$: C, 76.62; H, 5.56; N, 3.44. Found: C, 75.89; H, 5.58; N, 3.40.

[Pd(η^3-1,3-DiphenylC$_3$H$_3$)(py-2-CH=NMes)]PF$_6$ (4g(PF$_6$)): yellow solid, yield 45%. MALDI MS: 523.1 (M^+).

[Pd(η^3-1,3-DiphenylC$_3$H$_3$)(py-2-CH=NMes)]BPh$_4$ (4g(BPh$_4$)): yellow solid, yield 71%. Anal. Calcd for $C_{54}H_{49}N_2BPd$: C, 76.92; H, 5.86; N, 3.32. Found: C, 76.34; H, 6.08; N, 3.34.

[Pd(η^3-1,3-DiphenylC$_3$H$_3$)(py-2-CH=NMes)]BArF (4g(BArF)): yellow solid, yield 56%. Anal. Calcd for $C_{63}H_{47}N_2BF_{24}Pd$: C, 53.85; H, 3.37; N, 1.99. Found: C, 54.12; H, 3.18; N, 2.12.

[Pd(η^3-1,3-DiphenylC$_3$H$_3$)(py-2-CH=NC$_6$H$_4$(i-Pr)$_2$-2,6)]PF$_6$ (4h(PF$_6$)): yellow solid, yield 67%. MALDI MS: 565.2 (M^+).

[Pd(η^3-1,3-DiphenylC$_3$H$_3$)(py-2-CH=NC$_6$H$_4$(i-Pr)$_2$-2,6)]BPh$_4$ (4h(BPh$_4$)): yellow solid, yield 83%. Anal. Calcd for $C_{57}H_{55}N_2BPd$: C, 77.33; H, 6.26; N, 3.16. Found: C, 76.79; H, 6.54; N, 3.23.

[Pd(η^3-1,3-DiphenylC$_3$H$_3$)(py-2-CH=NC$_6$H$_4$(i-Pr)$_2$-2,6)]BArF (4h(BArF)): yellow solid, yield 62%. Anal. Calcd for $C_{65}H_{47}N_2BF_{24}Pd$: C, 54.62; H, 3.31; N, 1.96. Found: C, 54.66; H, 3.38; N, 2.11.

Acknowledgment. P.S.P. thanks the Swiss National Science Foundation and the ETH Zurich for support, as well as the Johnson Matthey Company for the loan of palladium salts. The support and sponsorship by COST Action D24 "Sustainable Chemical Processes: Stereoselective Transition Metal-Catalysed Reactions" is kindly acknowledged. A.A. thanks MIUR for support (PRIN 2007). B.F. thanks Ministerio de Ciencia y Técnología of Spain (CTQ: 2004-07667) for studentships.

Supporting Information Available: Scheme S1, Table S1, Figure S1, and Figures S2−5 with the energy profiles calculated for allyl rotation and for aryl rotation in complexes **4g** and **4h**, respectively, and Table S2 with atomic coordinates of all optimized structures. Experimental details and a full listing of crystallographic data, including tables of positional and isotropic equivalent displacement parameters, anisotropic displacement parameters, calculated positions of the hydrogen atoms, bond distances, bond angles, and torsional angles, are listed in the CIF file. This material is available free of charge via the Internet at http://pubs.acs.org.